Structural Characterization of Synthetic and Protein-Bound Porphyrins in Terms of the Lowest-Frequency Normal Coordinates of the Macrocycle

Walter Jentzen,* Xing-Zhi Song, and John A. Shelnutt*

Catalysis and Chemical Technologies Department, Sandia National Laboratories, Albuquerque, New Mexico 87185-0710, and Department of Chemistry, University of New Mexico, Albuquerque, New Mexico 87131

Received: October 14, 1996; In Final Form: December 2, 1996[⊗]

The X-ray crystal structures of synthetic and protein-bound metalloporphyrins are analyzed using a new normal structural decomposition method for classifying and quantifying their out-of-plane and in-plane distortions. These distortions are characterized in terms of equivalent displacements along the normal coordinates of the D_{4h}-symmetric porphyrin macrocycle (normal deformations) by using a computational procedure developed for this purpose. Often it turns out that the macrocyclic structure is, even in highly distorted porphyrins, accurately represented by displacements along only the lowest-frequency normal coordinates. Accordingly, the macrocyclic structure obtained from just the out-of-plane normal deformations of the saddling (*sad*, B_{2u})-, ruffling (*ruf*, B_{1u})-, doming (*dom*, A_{2u})-, waving [*wav*(*x*), *wav*(*y*); E_g]-, and propellering (*pro*, A_{1u})-type essentially simulates the out-of-plane distortion of the X-ray crystal structure. Similarly, the observed in-plane distortions are decomposed into in-plane normal deformations corresponding to the lowest-frequency vibrational modes including macrocycle stretching in the direction of the *meso*-carbon atoms (*meso-str*, B_{2g}), stretching in the direction of the nitrogen atoms (*N-str*, B_{1g}), *x* and *y* pyrrole translations [*trn*(*x*), *trn*(*y*); E_u], macrocycle breathing (*bre*, A_{1g}), and pyrrole rotation (*rot*, A_{2g}). The finding that the displacements of the 24 atoms of the macrocycle primarily occur along the lowest-frequency normal coordinates is expected on physical grounds and is verified by structural decomposition of more than 100 synthetic and 150 protein-bound metalloporphyrin X-ray crystal structures. Because of the high resolution of the X-ray crystal structures of synthetic metalloporphyrins, the small displacements for other normal coordinates are also able to be discerned. However, for the heme groups in proteins, only the displacements along the lowest-frequency modes are detectable because of the large uncertainties in the atomic positions. The heme groups in the four X-ray crystal structures of deoxyhemoglobin are used to evaluate the structural decomposition method. We find that the corresponding heme groups in different X-ray crystal structures are similar. Furthermore, the out-of-plane distortions for the heme groups in the α- and *β*-chains are found to be inequivalent, that is, the two α-heme groups are mainly ruffled and domed whereas the two *β*-heme groups are primarily saddled and domed. In the case of isozyme-1 ferrocytochrome *c* and its mutants, the heme distortion is not significantly influenced by the point mutations, and the strongly nonplanar structure is most likely the result of interactions of the heme group with a small protein segment, probably the linkage Cys−Leu−Gln−Cys−His. This conclusion is in agreement with previous findings that the heme distortion in cytochrome *c* is conserved for the proteins for which X-ray crystal structures exist and significant structural variation occurs only when an amino acid difference appears in Cys−X−Y−Cys−His segment. A similar conclusion is suggested by the structural decomposition results of the four heme groups in cytochromes c_3. The analogous covalently linked peptide segments vary for each heme group, giving different distortions for the four hemes. Nevertheless, the distinctive distortion of each heme group is conserved for cytochromes c_3 from different species as long as the short peptide sequences between the cysteine linkages are homologous.

Introduction

The possible biological significance of nonplanar porphyrin structures in proteins has long been recognized.[1] For example, biological properties like redox potential,[1a,b,2,3] axial ligation,[2] and UV−visible absorption[4−7] depend on the degree of nonplanarity. Specifically for hemoproteins, it has been reported that proton binding of particular amino acid residues changes the ligand affinity (Bohr effect) by inducing distortion of the heme groups in oxyhemoglobin.[8] Although the functional significance is unknown, a large nonplanar heme distortion is found in crystal structures of the mitochondrial cytochromes *c*.[9] This distortion is conserved in the proteins from different species.[10] The possible importance of nonplanar heme structures in a variety of proteins is further amplified by the observation that the heme is nonplanar only if the protein exerts substantial forces on the heme group. That is, in the absence of the protein environment (*e.g.*, in solution) the heme group is almost planar.[11]

Because of these recent findings, we decided to analyze the crystal structures of hemoproteins with the goal of classifying and quantifying the heme distortions. However, the asymmetric heme environment induces an overall distortion that cannot be characterized easily, and therefore, a simple and sensitive means of measuring the heme distortion is necessary.

In a previous paper,[7] a qualitative framework for classifying the out-of-plane distortions in terms of equivalent displacements along the lowest-frequency out-of-plane normal coordinates of the porphyrin macrocycle is described. This classification scheme is based on the observation that the out-of-plane distortions are often similar to static displacements along the lowest-frequency out-of-plane normal coordinates of the mac-

* Authors to whom correspondence should be addressed.

[⊗] Abstract published in *Advance ACS Abstracts,* February 1, 1997.

S1089-5647(96)03142-2 CCC: $14.00

rocycle. For example, the commonly observed out-of-plane distortions observed for the X-ray crystal structures of symmetrically substituted metalloporphyrins are ruffling (B_{1u}), saddling (B_{2u}), and doming (A_{2u}),[7] each resembling static displacements along the corresponding lowest-frequency normal coordinates of these symmetry types.[12]

The purpose of this work is to extend and refine this framework for describing the distortions of the porphyrin macrocycle. This goal has been accomplished by developing a computational procedure for measuring the out-of-plane and in-plane displacements along the normal-mode coordinates. In developing this procedure, normal-mode calculations on the assumed D_{4h}-symmetric macrocycles were carried out using a new force field capable of predicting most porphyrin X-ray crystal structures.[13] The resulting normalized eigenvectors (normal deformations) provide an almost orthogonal basis when transformed from the root-mass-weighted coordinate (displacement) system to the coordinate space. Displacements along these normal deformations are determined for the macrocyclic distortions of more than 100 synthetic and 150 protein-bound metalloporphyrin X-ray crystal structures. From these data, we verify the physically reasonable supposition that the displacements of macrocyclic atoms are primarily along the lowest-frequency normal coordinates. That is, in most cases the distortions are described adequately by summing only six out-of-plane normal deformations [*sad, ruf, dom, wav*(*x*), *wav*(*y*), *pro*] and six in-plane normal deformations [*m-str* (B_{2g}), N-*str* (B_{1g}), *trn*(*x*) (E_u), *trn*(*y*) (E_u), *bre* (A_{1g}), *rot* (A_{2g})] corresponding to the lowest-frequency normal modes of each symmetry type. Analysis of the structural decomposition results reveals new information concerning the heme groups in proteins, information previously hidden in the complicated heme distortions caused by the asymmetric heme environment.

Theoretical Approach

Recently, we noticed that the common types of nonplanar distortions of symmetrically substituted metalloporphyrins observed in X-ray crystal structures, such as the *ruf* and *sad* deformations defined by Scheidt and Lee,[14] closely match static displacements along the lowest-frequency normal coordinates of the macrocycle.[7] The reason that displacements of the 24 atoms of the macrocycle frequently occur along these out-of-plane normal coordinates is simply that these modes are the softest for distortion of the porphyrin. That is, they require the least energy, for example, to relieve steric interactions resulting from bulky substituents at the porphyrin periphery. Seeking a simple method to measure these distortions, we have now developed a mathematical procedure for characterizing the structure of porphyrins in terms of equivalent displacements along the out-of-plane and in-plane normal coordinates. This approach is a particularly useful way of describing the distortions of porphyrins because of the unique relationship between the normal-mode coordinates and molecular deformation energies.

Normal-Mode Calculation. In general, the internal atomic displacements of every molecule can be described exactly by specifying the static displacements along all of its normal-mode coordinates. In our case, we want to characterize the internal atomic displacements of the 24-atom porphyrin macrocycle ($C_{20}N_4$) by using the 66 modes corresponding to its 66 internal degrees of freedom ($3N - 6$). Assuming a planar D_{4h}-symmetric metalloporphyrin skeleton, the internal displacements are separated into out-of-plane and in-plane displacements. Specifically, the 66 vibrational modes split into 21 ($= N - 3$) out-of-plane (oop) and 45 ($= 2N - 3$) in-plane (ip) modes and are classified according to the irreducible representations of the D_{4h} point group as

$$\Gamma_{oop} = 2A_{1u} + 3A_{2u} + 3B_{1u} + 3B_{2u} + 5E_g$$

$$\Gamma_{ip} = 6A_{1g} + 5A_{2g} + 6B_{1g} + 6B_{2g} + 11E_u \qquad (1)$$

These normal-mode coordinates and their vibrational frequencies for each irreducible representation Γ listed in eq 1 are determined by solving the secular equation given by eq 2 in the root-mass-weighted coordinate displacement system.[15]

$$|\mathbf{M}^{-1/2}(\nabla^2 E)\,\mathbf{M}^{-1/2} - \lambda\mathbf{I}| = |\frac{1}{\sqrt{m_i m_j}}\frac{\partial^2 E}{\delta x_i \delta x_j} - \lambda\delta_{ij}| = 0 \qquad (2)$$

In this equation, the matrix $\nabla^2 E$ is called the Hessian matrix, the symbols **M** and **I** represent the diagonal mass matrix and the unit matrix, respectively, and δ_{ij} is the Kronecker delta symbol. The eigenvectors $\hat{\mathbf{Q}}_m^\Gamma$ (normal modes) corresponding to the eigenvalue λ_m^Γ of the *m*th mode of symmetry Γ are determined by diagonalization of the root-mass-weighted matrix of the second derivatives of the potential energy function *E* with respect to the Cartesian coordinates x_i. In the notation used, the variable *m* goes from 1,2, ... N_Γ arranged in the order of increasing vibrational frequencies and the symbol N_Γ is the number of the normal modes of symmetry type Γ. For example, $\hat{\mathbf{Q}}_1^{B1u}$ is the lowest-frequency normal mode of symmetry B_{1u}, and N_Γ is seen to be equal to 3 in eq 1. The normal-mode coordinates $\hat{\mathbf{Q}}_m^\Gamma$ span a 66-dimensional orthonormal space in the root-mass-weighted coordinate displacement system; that is, the dot products[16] between the eigenvectors are $\hat{\mathbf{Q}}'^\Gamma_m\hat{\mathbf{Q}}_k^\Gamma = \delta_{mk}^\Gamma$ (the prime indicates the transpose of the vector). The eigenvalues λ_m^Γ are proportional to the squares of the vibrational frequencies $\tilde{\nu}_m^\Gamma$ (in cm^{-1}). The normal-mode coordinates and their corresponding frequencies were computed by using the program POLYGRAPH (Molecular Simulation Inc.) for energy-minimized structures also obtained with POLYGRAPH.[6,7,13,17,18] This calculation is based on a recently developed new force field capable of accurately reproducing most porphyrin X-ray crystal structures.[13]

Normal Deformations. For the purpose of structurally decomposing known porphyrin X-ray crystal structures, the atomic coordinates of which are in the coordinate space, the root-mass-weighted normal coordinates $\hat{\mathbf{Q}}_m^\Gamma$ were transformed into the center of coordinate displacement system. In detail, the displacement coordinates $\mathbf{C}_m^\Gamma$ of the 24 macrocyclic atoms with respect to the center of mass are given by the transformation $\mathbf{C}_m^\Gamma = \mathbf{M}^{-1/2}\hat{\mathbf{Q}}_m^\Gamma$. These coordinates $\mathbf{C}_m^\Gamma$ are then translated to the center of atomic coordinate displacement system, and in addition, the rigid-body rotations of each eigenvector are also removed to obtain solely the actual internal displacement vectors. (The mathematical procedure is described in Appendix A available in the Supporting Information.) Removing the translational and rotational contributions only alters the E_u, A_{2u} and E_g, A_{2g} modes since they transform like translations and rotations in D_{4h} symmetry, respectively. In this work, the transformed eigenvectors defined in the center of atomic coordinate displacement system are called normal deformations and are designated by the symbols $\hat{\mathbf{D}}_m^\Gamma$. They are normalized by requiring $\sqrt{\hat{\mathbf{D}}'^\Gamma_m\hat{\mathbf{D}}_m^\Gamma} = |\hat{\mathbf{D}}_m^\Gamma| = 1$ in which the double bars represent the norm of the vector $\hat{\mathbf{D}}_m^\Gamma$. It must be kept in mind that these normal deformations are not quite orthogonal within a symmetry type because the masses of the nitrogen and carbon atoms are slightly different.

Thus, the basis set used for decomposing the structures of porphyrins consists of 66 normal deformations $\hat{\mathbf{D}}_m^\Gamma$, resulting from the normal-mode calculation of the planar macrocycle.

The selection and calculation of this planar macrocycle are thoroughly discussed in the Results and Discussion section. The normal deformations $\hat{\mathbf{D}}_m^\Gamma$ are then simply 1-Å displacements in the coordinate space from their equilibrium position for each of the normal coordinates. The elements of the normal-deformation vector are made up of the individual coordinate displacement $\Delta\hat{\vec{r}}_n$ for each of the 24 atoms of the macrocycle. (Figure S1 in the Supporting Information shows the customary used atomic labeling scheme.) The $\Delta\hat{x}_n$ and $\Delta\hat{y}_n$ components are zero for all atoms for the out-of-plane normal deformations, and the $\Delta\hat{z}_n$ components are zero for the in-plane normal deformations.

Observed Distortion and the Reference Macrocyclic Structure. The displacement vectors $\Delta\hat{\vec{r}}_n$ are relative quantities; consequently, before decomposing the structures of porphyrins, we first need the observed displacement coordinates of each macrocyclic atom $(\Delta\hat{\vec{r}}_n)_{obs}$ of the structure to be decomposed. This requires an assumed D_{4h}-symmetric reference structure $\mathbf{S}_{ref}$. The selection of this reference structure is discussed in the Results and Discussion section. Using the atomic coordinates of the reference structure, the observed distortion $\mathbf{D}_{obs}$ of the 24 macrocyclic atoms is then defined by eq 3

$$\mathbf{D}_{obs} = \mathbf{S}_{obs} - \mathbf{S}_{ref} \tag{3}$$

The symbol $\mathbf{S}_{obs}$ represents the observed structure, consisting of the observed X-ray atomic coordinates of the 24 atoms of the macrocycle. The reference structure is really only required for describing the observed in-plane displacements. In contrast, the observed out-of-plane distortions are solely given by the observed structure $\mathbf{S}_{obs}$. That is, the out-of-plane distortions are defined by giving the observed Δz displacements of the atoms with respect to the least-squares (mean) plane. Thus, the mean plane ($\Delta z = 0$) is the reference for the out-of-plane distortion.

In particular, there are two steps involved in determining the observed displacement vector $(\Delta\hat{\vec{r}}_n)_{obs}$ of the nth macrocyclic atom. First, the calculation of the mean plane defined by the X-ray atomic coordinates of the observed structure $\mathbf{S}_{obs}$ ultimately gives the out-of-plane displacements (Δz components of $\mathbf{S}_{obs}$) of the macrocyclic atoms after transformation of the xy-plane of the coordinate system into this mean plane. The basic method for calculating a mean plane to a set of points has already been reported by Schomaker and co-workers.[19] Second, only a final z-axis rotation is necessary to best match up the observed x, y atomic coordinates to the x, y atomic coordinates of the reference structure $\mathbf{S}_{ref}$. This mathematical procedure defines the in-plane displacements (Δx and Δy components of $\mathbf{D}_{obs}$) of the macrocyclic atoms. Both the determination of the mean plane and the final z-axis rotation are based on a least-squares method, and the mathematical procedure is described in Appendix B, available in the Supporting Information.

Structural Decomposition of the Observed Structure. We characterize the observed structures of porphyrins by decomposing the observed displacement coordinates into equivalent displacements along the normal coordinates (normal deformations). In other words, the observed displacements of the 24 macrocyclic atoms of an X-ray structure are described as a linear combination of the vibrational (harmonic) eigenvectors in the coordinate space

$$\mathbf{D}_{obs} = \sum_{\Gamma,m} d_m^\Gamma \hat{\mathbf{D}}_m^\Gamma \cos(2\pi c \tilde{\nu}_m^\Gamma t + \varphi_m^\Gamma) \tag{4}$$

The symbol d_m^Γ (in angstroms) is the (scalar) displacement along the normal coordinates, $\tilde{\nu}_m^\Gamma$ is the vibrational frequency (in cm^{-1}) of the normal mode, and c the velocity of light. For static description, the time t and the phases φ_m^Γ can be set to be zero for each eigenvector. In addition, the observed displacements are separated into out-of-plane and in-plane contributions which gives the following equation:

$$\mathbf{D}_{obs} = \sum_{\Gamma,m} d_m^\Gamma \hat{\mathbf{D}}_m^\Gamma = \sum_{\Gamma_{oop},m} d_m^{\Gamma_{oop}} \hat{\mathbf{D}}_m^{\Gamma_{oop}} + \sum_{\Gamma_{ip},m} d_m^{\Gamma_{ip}} \hat{\mathbf{D}}_m^{\Gamma_{ip}} = \mathbf{D}_{obs}^{oop} + \mathbf{D}_{obs}^{ip} \tag{5}$$

The structure is then characterized by determining the displacement along each normal deformation, given by the displacements d_m^Γ. Accordingly, the whole set of displacements d_m^Γ characterizes the observed structure, and each displacement d_m^Γ gives the contribution of the normal deformation $\hat{\mathbf{D}}_m^\Gamma$ to the total observed distortion. These displacements are obtained by multiplying eq 5 with the transpose of the vector $\hat{\mathbf{D}}_j'^\Gamma$ (using the fact that $\hat{\mathbf{D}}_j'^\Gamma \hat{\mathbf{D}}_m^\Lambda = 0$ if $\Gamma \neq \Lambda$):

$$d_m^\Gamma = \sum_{k=1}^{N_\Gamma} \bar{B}_{mk}^\Gamma P_k^\Gamma \tag{6}$$

with $\bar{\mathbf{B}}^\Gamma = (\mathbf{B}^\Gamma)^{-1}$, where $B_{jm}^\Gamma = \hat{\mathbf{D}}_j'^\Gamma \hat{\mathbf{D}}_m^\Gamma$ and $P_j^\Gamma = \hat{\mathbf{D}}_j'^\Gamma \mathbf{D}_{obs}$.

The number of symmetric square matrices $\mathbf{B}^\Gamma$ is determined by the number of different irreducible representations Γ, and its dimension is determined by the number of modes belonging to the same irreducible representations given by N_Γ. For instance, $\mathbf{B}^{B1u}$ is a (3×3) matrix according to eq 1.

In spectroscopy, it is of interest to know the overall displacements along the normal coordinates of each symmetry type Γ. To obtain this quantity, eq 5 can be rearranged so that the observed distortion is separated into the overall deformations $\mathbf{D}_{obs}^\Gamma$ of each symmetry type Γ:

$$\mathbf{D}_{obs} = \sum_\Gamma \mathbf{D}_{obs}^\Gamma, \text{ where } \mathbf{D}_{obs}^\Gamma = \sum_{m=1}^{N_\Gamma} d_m^\Gamma \hat{\mathbf{D}}_m^\Gamma \tag{7}$$

The magnitude is given by eq 8:

$$D_{obs}^\Gamma = |\mathbf{D}_{obs}^\Gamma| = \sqrt{\sum_{k,j=1}^{N_\Gamma} B_{kj}^\Gamma d_k^\Gamma d_j^\Gamma} \tag{8}$$

Thus, the set of displacements d_m^Γ for modes of the same symmetry type Γ determines the magnitude of the total deformation of each symmetry type.

It is obvious that the total magnitude of distortion is also a useful quantity for characterizing the observed structures. Given the individual displacement coordinates of the 24 atoms of the observed structure, the magnitude of the total distortion D_{obs} (in angstroms) is defined by eq 9 and is separated into out-of-plane D_{obs}^{oop} and in-plane D_{obs}^{ip} contributions, each defined by eq 10 and 11, respectively.

$$D_{obs} = |\mathbf{D}_{obs}| = \sqrt{\sum_{n=1}^{24} (\Delta\vec{r}_n)_{obs}^2} = \sqrt{(D_{obs}^{oop})^2 + (D_{obs}^{ip})^2} \tag{9}$$

$$D_{obs}^{oop} = |\mathbf{D}_{obs}^{oop}| = \sqrt{\sum_{n=1}^{24} (\Delta z_n)_{obs}^2} \tag{10}$$

$$D^{ip}_{obs} = |\mathbf{D}^{ip}_{obs}| = \sqrt{\sum_{n=1}^{24} (\Delta x_n)^2_{obs} + (\Delta y_n)^2_{obs}} \quad (11)$$

Reduced Basis. After decomposing the observed structures of synthetic and protein-bound porphyrins according to the above procedure, it turns out that in many cases the distortions of various metalloporphyrins can be described adequately with only 12 or less normal deformations $\hat{\mathbf{D}}^{\Gamma}_1$ (*vide infra*). That is, only the corresponding lowest-frequency normal modes of each symmetry type are required to simulate the structures. We call this basis set the *minimal* basis ($m = 1$). Because of the high-resolution of the X-ray crystal structures of synthetic metalloporphyrins, the small displacements of other normal coordinates are also able to be discerned. For example, the displacements of the second lowest-frequency normal coordinates of each symmetry type can be included with the minimal basis to give an *extended* basis ($m \leq 2$), and using the extended basis significantly improves the agreement between the simulated and observed structures for the synthetic porphyrins. In the case of the heme groups in proteins, however, only the displacements along the lowest-frequency modes (minimal basis) are discernible because of the large uncertainties in the atomic positions.

Simulated Structures Using the Minimal Basis. In the minimal basis, the symmetry of each of the 6 in-plane and 6 out-of-plane normal deformations is different; therefore, these normal deformations span an orthonormal 12-dimensional coordinate space. In this case, the solution of the corresponding displacements d^{Γ}_1 is simply given by ($\mathbf{B}^{\Gamma} = 1$) eq 12:

$$d^{\Gamma}_1 = P^{\Gamma}_1 = \hat{\mathbf{D}}'^{\Gamma}_1 \mathbf{D}_{obs}, \Gamma = \Gamma_{ip} + \Gamma_{oop} \quad (12)$$

Naturally, since this 12-dimensional space does not span the full 66-dimensional coordinate space, the simulated distortion based on just these 12 displacements

$$\mathbf{D}_{sim,1} = \sum_{\Gamma} d^{\Gamma}_1 \hat{\mathbf{D}}^{\Gamma}_1 = \sum_{\Gamma_{oop}} d^{\Gamma_{oop}}_1 \hat{\mathbf{D}}^{\Gamma_{oop}}_1 + \sum_{\Gamma_{ip}} d^{\Gamma_{ip}}_1 \hat{\mathbf{D}}^{\Gamma_{ip}}_1 = \mathbf{D}^{oop}_{sim,1} + \mathbf{D}^{ip}_{sim,1} \quad (13)$$

will not exactly match the observed structure. Also, the magnitude of this simulated total distortion

$$D_{sim,1} = |\mathbf{D}_{sim,1}| = \sqrt{(D^{oop}_{sim,1})^2 + (D^{ip}_{sim,1})^2} \quad (14)$$

will not exactly equal the observed total distortion given by eq 9. In eq 14, $D^{oop}_{sim,1}$ and $D^{ip}_{sim,1}$ are the simulated out-of-plane and in-plane distortions, respectively, using only the minimal basis, that is

$$D^{oop}_{sim,1} = |\mathbf{D}^{oop}_{sim,1}| = \sqrt{\sum_{\Gamma_{oop}} (d^{\Gamma_{oop}}_1)^2} \quad (15)$$

$$D^{ip}_{sim,1} = |\mathbf{D}^{ip}_{sim,1}| = \sqrt{\sum_{\Gamma_{ip}} (d^{\Gamma_{ip}}_1)^2} \quad (16)$$

Estimation of the Goodness of the Simulated Structures. Since the minimal basis does not give an exact agreement between the observed and simulated distortion, we need a measure of the goodness of the simulated distortion. Either the mean positional deviation or the root-mean-square (rms) deviation is a suitable quantity. In X-ray protein crystallography, the mean positional error is commonly used[20] and serves in our case as a criterion for comparison with the goodness-of-fit parameter for the simulated structure. Thus, in our case, we choose the mean deviations (in angstroms) in one ($\bar{\delta}_{oop,1}$) and two dimensions ($\bar{\delta}_{ip,1}$) as a measure of the goodness-of-fit. These quantities are given by eq 17:

$$\bar{\delta}_{oop,1} = {}^1/_{24} \sum_{n=1}^{24} \sqrt{[(\Delta z_n)_{sim,1} - (\Delta z_n)_{obs}]^2}$$

$$\delta_{ip,1} = {}^1/_{24} \sum_{n=1}^{24} \sqrt{[(\Delta x_n)_{sim,1} - (\Delta x_n)_{obs}]^2 + [(\Delta y_n)_{sim,1} - (\Delta y_n)_{obs}]^2} \quad (17)$$

These deviations should be compared to the mean positional errors in X-ray crystallography for the proteins. However, for the synthetic porphyrins the positional uncertainties are given in terms of the rms errors, and thus should be compared to the rms deviation between simulated and observed structures. In Appendix C of the Supporting Information, under certain conditions the rms deviation in different dimensions is shown to be almost the same as the mean deviation given above.

The structural decomposition method can be readily applied if the observed distortion $\mathbf{D}_{obs}$ ($= \mathbf{S}_{obs} - \mathbf{S}_{ref}$) and the normal deformations $\hat{\mathbf{D}}^{\Gamma}_m$ are known. The appropriate selection of the reference structure $\mathbf{S}_{ref}$ and the eigenvectors $\hat{\mathbf{Q}}^{\Gamma}_m$ (and hence $\hat{\mathbf{D}}^{\Gamma}_m$) is discussed in the next section.

Results and Discussion

Structural Decomposition of Metalloporphyrin X-ray Crystal Structures. The description of the distortion of a porphyrin in terms of equivalent displacements along the normal coordinates provides a uniquely useful framework for classifying and quantifying porphyrin structures. This description occupies a special position relative to other equivalent descriptions. For example, for the out-of-plane distorted structures, one might give a listing of Δz displacements with respect to the mean plane or specify the macrocyclic torsion angles. The uniqueness of the description in terms of normal deformations results from the simple relationship between the macrocyclic deformation energies and the displacements along the normal coordinates. In detail, the total distortion energy is just the sum of contributions from each normal deformation type. As a result, if the displacement along each normal coordinate is known, then the total energy and the contribution of each deformation type can be simply estimated (*vide infra*). In addition, a great simplification in the description of the distortion occurs when expressed in the normal-deformation space. This is because typically only a few of the lowest-frequency normal coordinate contribute substantially to the distortions of porphyrins. Most importantly, by using the normal coordinates to characterize the complicated distortions of porphyrins in proteins, we are more likely to discover possible relationships among the molecular structures, spectroscopic features, and biological functions.

For these reasons, we devised the computational procedure described above to determine the displacements along the normal coordinates for the structures of any distorted porphyrin. These macrocyclic distortions can occur for a variety of reasons including bulky substituents at the porphyrin periphery,[5,6,17] small or too large metal ions in the porphinato core,[17b,21] axial ligands,[14,22] and a multitude of interactions with the environment, *e.g.*, protein−heme interactions in hemoproteins.[2,10,23] In the past, the structural quantification of these distortions, sometimes composed of a complicated combination of normal deformations, was usually accomplished by eye in approximate fashion.

The structural decomposition method described here uniquely projects out the contribution of each symmetric normal deformation type to the total distortion, providing a precise quantitative measure of the structure. This method has already been applied successfully for describing the out-of-plane distortions observed in X-ray crystal and energy-minimized structures of synthetic metalloporphyrins.[13,24] Moreover, the method is especially useful for characterizing the complicated distortion of the heme groups in proteins.

Before decomposing synthetic and protein-bound metalloporphyrin X-ray crystal structures using the structural decomposition method, we first have to select judiciously the structure $\mathbf{S}_{ref}$ to which the observed distortions of the 24 atoms of the macrocycle are referenced. In addition, we have to determine the normal-mode coordinates $\hat{\mathbf{Q}}_m^{\Gamma}$ and hence the normal deformations $\hat{\mathbf{D}}_m^{\Gamma}$ along which the observed macrocyclic distortion will be decomposed.

Selection of the Reference Structure and Determination of the Normal Deformations. The selection of the D_{4h}-symmetric reference structure should consider the fact that the internal strains should be as small as possible. On the one hand, a planar and less strained porphyrin is favored by hydrogen atoms as peripheral substituents; therefore, a metalloporphine is a good choice. On the other hand, the in-plane strain is a minimum if the metal ion is not too small and too large. Otherwise, the metal leads to internal strains resulting in in-plane and out-of-plane distortions of the macrocycle. The optimum metal−nitrogen distance for planar metalloporphyrins that is thought to be about 2.01 Å.[25] Upon comparing the metal−nitrogen distances of recently crystallized X-ray crystal structures of metalloporphines M(P)[26] [M: Ni(II),[26b] Co(II), Cu(II), Zn(II)], the geometry of copper(II) porphine [Cu(P)] best fulfills the condition (Ct−N distance 1.998 Å). Consequently, the symmetry-adapted atomic coordinates of Cu(P) obtained from the X-ray crystal structure were selected as the reference structure in the simulations. (The coordinates of this planar structure are listed in Table S2 in the Supporting Information.) After selecting this reference structure, the observed displacement coordinates of the 24 atoms of the macrocycle summarized in the $\mathbf{D}_{obs}$ are now defined by using the computational procedure given in the Appendix B in the Supporting Information.

Finally, we need the 66 linearly independent eigenvectors of the normal deformations. These are obtained from a normal-mode calculation on the 24-atom macrocycle ($C_{20}N_4$); however, the central metal ion, copper(II), should be retained formally to keep the interior binding geometry that of a metalloporphyrin. The assumed 25-atom porphyrin macrocycle including the metal has 69 eigenvectors for describing 66 internal degrees of freedom of the macrocycle. This leads to ambiguities in the normal deformations if only the macrocyclic atoms are considered.[27] In order to avoid these ambiguities, we set the mass of the metal to nearly zero (0.001 amu) in the normal-mode calculation, resulting in an almost complete separation of the motion of the metal and the macrocycle. [This mode separation occurs naturally for the CH stretches (3000-cm^{-1} region) and the modes of the macrocycle (<1700 cm^{-1}) of metalloporphines.] By setting the mass of copper to almost zero, the three modes of A_{2u} and E_u symmetry exhibiting large metal motion appear at very high frequencies (>30 000 cm^{-1}) and have been omitted in our basis set for describing the distortion of the macrocycle. Furthermore, setting the mass of the metal to nearly zero still leads to small metal displacements in the root-mass-weighted coordination displacement system for some A_{2u} and E_u eigenvectors; these minute displacements were also neglected before transforming the eigenvectors into the center of coordinate displacement system. Omitting the ultra-high frequency modes leads to the necessary 66 linearly independent normal deformations $\hat{\mathbf{D}}_m^{\Gamma}$ making up the basis set used for decomposing the observed distortions of various metalloporphyrin macrocycles.

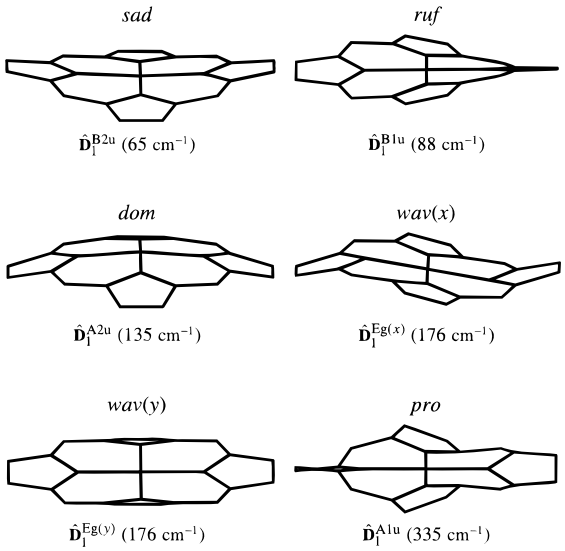

Figure 1. Illustrations of the lowest-frequency out-of-plane eigenvectors in the coordinate space, for each of the normal deformation $\hat{\mathbf{D}}_1^{\Gamma_{oop}}$ used in describing the nonplanar distortions of the porphyrin macrocycle. Static displacements representing a 1-Å deformation along each lowest-frequency normal coordinate are shown, and the metal is included for clarity.

Minimal Basis. The static 1-Å deformations along the lowest-frequency out-of-plane and in-plane normal-mode coordinates of each symmetry (minimal basis), representing the normal deformations $\hat{\mathbf{D}}_m^{\Gamma}$ in the coordinate displacement space, are shown in Figures 1 (out-of-plane) and 2 (in-plane) along with calculated vibrational frequencies and abbreviations used in this work. [In the Supporting Information, Figures S2 (out-of-plane) and S3 (in-plane) illustrate the normal deformations $\hat{\mathbf{D}}_2^{\Gamma}$ and $\hat{\mathbf{D}}_3^{\Gamma}$, and Tables S3 and S4 list the atomic displacement coordinates for the normal deformations $\hat{\mathbf{D}}_1^{\Gamma}$, $\hat{\mathbf{D}}_2^{\Gamma}$, and $\hat{\mathbf{D}}_3^{\Gamma}$.] The normal-mode eigenvectors giving these deformations are obtained from the normal-mode calculation on the copper macrocycle in its energy minimized planar geometry using the molecular mechanics force field.[13] In previous papers,[7,13] the 6 normal deformations $\hat{\mathbf{D}}_1^{\Gamma_{oop}}$ are called *sad* (B_{2u}), *ruf* (B_{1u}), *dom* (A_{2u}), *wav*(*x*), *wav*(*y*) (E_g), and *pro* (A_{1u}). The corresponding six in-plane normal deformations $\hat{\mathbf{D}}_1^{\Gamma_{ip}}$ have not been characterized yet, and in this work, they are referred to as *m-str* (B_{2g}), *N-str* (B_{1g}), *trn*(*x*), *trn*(*y*) (E_u), *bre* (A_{1g}), and *rot* (A_{2g}). As can be seen from Figure 2, the *m-str* (B_{2g}) and *N-str* (B_{2g}) deformation stretch the macrocycle along opposite methine bridges and pyrrole rings, respectively. The *trn* deformation (E_u) is doubly-degenerate and the displacement vectors of the pyrrole rings resemble translational deformations in *x* and *y* directions. The *bre* deformation (A_{1g}) is a macrocycle breathing deformation. Finally, each pyrrole ring in the *rot* deformation (A_{2g}) rotates in-phase (counterclockwise in Figure 2).

In most cases, the observed distortions of various metalloporphyrins can be described properly using only these 12 normal deformations shown in Figures 1 and 2 (*vide infra*). Consequently, the accuracy of these lowest-frequency normal modes is especially important. For this reason, we calculated the lowest-frequency normal coordinates and frequencies of Ni(P) using our molecular mechanics force field to compare with published data. We selected Ni(P) because it is structurally related to the copper−macrocycle reference structure and

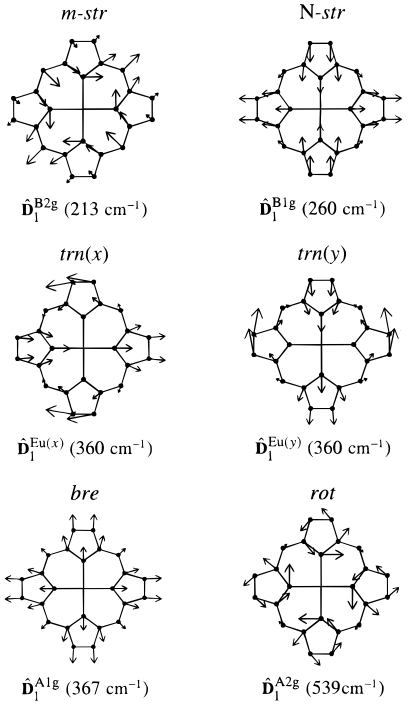

Figure 2. Illustrations of the lowest-frequency in-plane eigenvectors in the coordinate space, for each of the normal deformation $\hat{\mathbf{D}}_1^{\Gamma_{ip}}$ used in describing the in-plane distortions of the porphyrin macrocycle. The in-plane displacements represent a 1-Å deformation along each normal coordinate. For clarity, the atomic displacements shown are enlarged by a factor of 5 and the metal is included.

because there are spectroscopic data available. These comparisons are described in Appendix D of the Supporting Information.

Briefly, Table S6 in the Supporting Information lists the lowest-frequency in-plane and out-of-plane normal modes of nickel(II) porphine [Ni(P)] calculated with the molecular mechanics method and also those taken from other working groups using *ab initio* calculations,[28a] semiempirical force field methods,[28b] and normal coordinate analysis.[28c] The vibrational frequencies obtained with the molecular mechanics force field are in good agreement with those obtained with these other methods. Specifically, a comparison of the Raman-active in-plane displacement vectors of the lowest-frequency modes from Spiro and co-workers[28c] shows that the normal mode eigenvectors are almost the same as those calculated using molecular mechanics. Also, comparison of the atomic displacements of the macrocycle atoms for the low-frequency out-of-plane normal modes of nickel(II) octaethylporphyrin [Ni(OEP)] calculated by Li and co-workers[28d] shows good agreement with those of the corresponding modes used in the decomposition. This is as expected since the molecular mechanics force field is based on the normal coordinate analysis of Ni(OEP).[6,13] Altogether these results indicate that the lowest-frequency normal coordinates of the macrocycle that were used in the decomposition are reasonable.

In addition, the force field used to calculate the normal modes also predicts accurately the observed structure of Ni(P).[26b] The energy-minimized geometry of Ni(P) exhibits mean deviations from the corresponding X-ray crystal structure of 0.005 Å for bond distances and 0.3° for bond angles, respectively. Figure S4 in the Supporting Information compares the bond angles and distances of the X-ray crystal and energy-minimized structure of Ni(P).

The makeup of the normal coordinates might change when peripheral substituents are present. Thus, the influence of D_{4h}-symmetric substitution on the lowest-frequency normal coordinates was also investigated and is also described in Appendix D of the Supporting Information. It was found that the *relative* displacements of the macrocyclic atoms are almost identical with the normal deformations. Hence, symmetric substitution at the periphery has only a minor influence on the displacements for the lowest-frequency macrocyclic normal modes.

TABLE 1: Square of the Frequency Ratio of the Two Lowest-Frequency Normal Modes of the Macrocycle, Estimated Structural Changes in Bond Angles or Atomic Displacements, and Estimated Distortion Energies[a] for a 1-Å Distortion for Each Normal Deformation $\hat{\mathbf{D}}_1^{\Gamma}$. Energy Calculations Are Based on the Calculated Vibrational Frequencies $\tilde{\nu}_1^{\Gamma}$ of the Macrocycle

$(\tilde{\nu}_1^{\Gamma}/\tilde{\nu}_2^{\Gamma})^2$	$\hat{\mathbf{D}}_1^{\Gamma}$	change in bond angle or atomic displacement		K_1^{Γ} (kJ mol^{-1} Å^{-2})
0.064	B_{2u} (*sad*)	Δ(N−Ct−N)[b]	4.2 deg Å^{-1}	9.1
0.029	B_{1u} (*ruf*)	C_αN−NC_α[c]	22.0 deg Å^{-1}	16.5
0.141	A_{2u} (*dom*)	Δ(N−It−N)[d]	32.2 deg Å^{-1}	41.4
0.547	E_g (*wav*)	pyrrole tilting[e]	36.9 deg Å^{-1}	67.3
0.243	A_{1u} (*pro*)	C_αN−NC_α[f]	25.9 deg Å^{-1}	238.4
0.248	B_{2g} (*m-str*)	C_m stretching[g]	0.284	100.1
0.118	B_{1g} (*N*-str)	N stretching[g]	0.193	147.8
0.760	E_u (*trn*)	N translation[g]	0.227	280.5
0.274	A_{1g} (*bre*)	N breathing[g]	0.200	293.8
0.491	A_{2g} (*rot*)	N rotation[g]	8.2 deg Å^{-1}	652.9

[a] Value of K_1^{Γ} corresponds to the energy (in kJ mol^{-1}) of a 1-Å distortion. Calculation assumes that the bond distances of the distorted structure are almost equal to the planar reference structure. [b] Change of the angle N−Ct−N from 180° [$\sin(0.5\theta) = -0.037(d_1^{B2u}/\text{Å})$]. Symbol Ct represents the macrocycle center and the symbols N are the nitrogens of the opposite pyrroles. [c] Dihedral angle [$\sin(0.5\theta) = 0.191(d_1^{B1u}/\text{Å})$]. [d] Change of the angle N−It−N from 180° [$\sin(0.5\theta) = -0.277(d_1^{B2u}/\text{Å})$]. Position It is defined by the interception of the two extended lines coming from the opposite pyrroles of the *dom* conformation. Each line is defined by the average position of the two carbon atoms C_α and the nitrogen atom N of each pyrrole ring of the domed structure. [e] Tilting of the *x* or *y* pyrrole planes for the *wav*(*x*) or *wav*(*y*) deformation with respect to the mean plane [$\sin(\theta) = 0.600(d_1^{Eg}/\text{Å})$]. [f] Dihedral angle [$\sin(0.5\theta) = 0.224(d_1^{A1u}/\text{Å})$]. [g] Structural changes depend linearly on d_1^{Γ} except the angle θ for the N rotation [$\sin(\theta) = 0.142(d_1^{A2g}/\text{Å})$].

In previous work,[6,13,17,21] we used certain structural parameters to quantify the deformations of the minimal basis. It turns out that the displacements d_1^{Γ} are correlated with changes in these characteristic bond angles or atomic displacements. Table 1 summarizes the structural parameters selected as an alternative measure of each of the normal deformations. For example, the *sad* and *ruf* deformations are usually characterized by the tilt angle N−Ct−N and the dihedral angle C_αN−NC_α of the opposite pyrrole planes, respectively. From Table 1, a 1-Å *sad* deformation lowers the angle N−Ct−N by about 4.2° from 180° for the planar reference structure. Similarly, for a 1-Å *ruf* deformation, the dihedral angle C_αN−NC_α is 22.0°. For small displacements,[29] the structural parameters are linearly related to the size of the deformation with the proportionality factor given in Table 1.

Relationship Between the Distortion Energy and the Normal Deformation. The total energy required to induce a distortion defined by the displacements, along each normal deformation $\hat{\mathbf{D}}_m^{\Gamma}$, is given for small displacements from the equilibrium structure by eq 18:

$$V_{\text{tot}} = \sum_{\Gamma,m} V(d_m^{\Gamma}) = 2\pi^2 c^2 \sum_{\Gamma,m} (\tilde{\nu}_m^{\Gamma})^2 (\mathbf{Q}_m^{\Gamma})^2 = \sum_{\Gamma,m} K_m^{\Gamma} (d_m^{\Gamma})^2 \quad (18)$$

where $\tilde{\nu}_m^{\Gamma}$ is the vibrational frequency (in cm^{-1}) of the *m*th normal mode of symmetry Γ and *c* the velocity of light. Only when the distortion is expressed in terms of the normal deformations, the total energy can be expressed as a single sum

of independent energy terms. The description of macrocyclic structures in terms of the normal deformations therefore occupies a unique position with respect to other descriptions. This is because typically only a few of the lowest-frequency normal coordinates contribute substantially to the distortions of porphyrins. Table 1 gives the energy necessary to generate a 1-Å deformation ($d_1^\Gamma = 1$ Å) for each of the modes of the minimal basis obtained by using the frequencies of the macrocyclic modes from the molecular mechanics calculations. This distortion energy is independent of the nature of the attached substituents, since the frequencies $\tilde{\nu}_m^\Gamma$ are the frequencies of the normal modes of the macrocycle.[30]

In this description, the deformation energy is proportional to the square of the vibrational frequencies according to eq 18. As a result, displacements along the lowest-frequency macrocyclic normal coordinates require the least energy to overcome perturbations upon the planar macrocycle. Hence, it is not surprising that distortion of symmetrically substituted metalloporphyrin X-ray crystal structures frequently resembles the normal deformations $\hat{\mathbf{D}}_1^\Gamma$, particularly the low-frequency *sad*, *ruf*, and *dom* deformations.[7] Their frequencies are the lowest; therefore, the restoring forces are the smallest. Thus, perturbations can easily cause distortions along these out-of-plane normal deformations for these modes. In the case of the in-plane distortions, we anticipate that the most probable asymmetric distortions are *m-str* (B_{2g}) and *N-str* (B_{1g}), whereas the *trn* (E_u) and especially *rot* (A_{2g}) are less likely. It is clear that the presence of the totally symmetric *bre* deformation (A_{1g}) depends on the reference structure selected, so its absolute value and even the necessity of $\hat{\mathbf{D}}_m^{A1g}$ ($m > 1$) are generally physically inconsequential. Similarly, the contribution of the *bre* deformation energy to the total distortion energy also depends on the reference structure, and consequently the *bre* deformation energy is also a relative quantity.

Structural Decomposition of X-ray Crystal Structures of Synthetic Porphyrins. The X-ray crystal structures of more than 100 synthetic metalloporphyrins, partly retrieved from the Cambridge Structural Database,[31] have been analyzed. Table 2 lists the out-of-plane and in-plane displacements d_1^Γ (minimal basis) of some selected X-ray crystal structures. (Table S5 in the Supporting Information lists displacements of the extended basis and the total deformations $\mathbf{D}_{obs}^\Gamma$ of each symmetry type Γ.) By examination of the results in Table 2 and Table S5, we find that most structures are well simulated using deformations along only a subset of the minimal-basis deformations. That is, the out-of-plane distortions of synthetic metalloporphyrins primarily occur along the *sad* (B_{2u}), *ruf* (B_{1u}), *dom* (A_{2u}), *wav*(*x*)- (E_g), and *wav*(*y*) (E_g) deformation types, and the common in-plane distortions are combinations of the *m-str* (B_{2g}), *N-str* (B_{1g}), and *bre* (A_{1g}) deformations (see Table 2). The *pro* (A_{1u}) and *rot* (A_{2g}) deformation types are practically absent. The reason that the *pro* and *rot* deformations are small is that these normal deformations require energetically large perturbations because of the high frequencies for these normal modes (*vide infra*). Also, the *trn*(*x*) and *trn*(*y*) (E_u) deformation types are remarkably small, probably because the structural perturbations causing these distortions of the compounds listed in Table 2 are not of the necessary symmetry.

The decomposition of the asymmetrically substituted nickel(II) 5,15-diphenyl-2,8,12,18-tetraethyl-3,7,13,17-tetramethylporphyrin[24] [Ni(dPTETMP)] is a good example of the usefulness of the unique description given by the structural decomposition method. Figure 3 shows the X-ray crystal structure of Ni(dPTETMP) and also the simulated structures generated from the projections of the out-of-plane and in-plane displacements along the lowest-frequency normal coordinates. The out-of-plane displacements are shown as a linear display of the macrocycle as is commonly used for illustrating nonplanar distortions. For the in-plane distortion, the arrows indicate the scaled displacements (enlarged by a factor of 15) with respect to the reference structure. The structure obtained using the minimal basis is superimposed on the X-ray structure, allowing the X-ray crystal and simulated structures to be visually compared. From Table 2, this asymmetric porphyrin exhibits a total observed and simulated nonplanar distortion of 1.219 and 1.211 Å, respectively. This distortion is decomposed into a −1.192 Å *sad* deformation and equal amounts 0.154 Å of *wav*(*x*) and *wav*(*y*) deformations. The total observed and simulated in-plane distortions are considerably smaller, 0.295 and 0.264 Å, respectively. Besides the predominant *m-str* deformation of −0.193 Å caused by the 5,15-phenyl substituents, we also identify smaller contributions of 0.034 Å of *trn*(*x*)- and *trn*(*y*) deformations. The *bre* deformation (−0.173 Å) is partly a result of the difference of the metals between Ni(dPTETMP) and the copper-macrocycle reference structure. The characteristic structural parameters associated with each normal deformation can be estimated using Table 1. For example, the presence of the *sad* deformation changes the tilt angle N−Ct−N by about 5° [= (4.2 deg Å^{-1}) × (1.192 Å)], and the *m-str* deformation involves displacements of the *meso* carbon atoms of the amount of 0.055 Å (= 0.284 × 0.193 Å). Under the condition that the potential energy is approximately harmonic (quadratic), the energy required to induce deformations of each type can also be estimated using the energy parameters (force constants), K_1^Γ, and the displacements, d_1^Γ, given in Tables 1 and 2, respectively. For instance, the macrocyclic energy for the *sad* deformation is 12.9 kJ mol^{-1} (= 9.1 × 1.192^2 kJ mol^{-1}) and for the *m-str* deformation 3.7 kJ mol^{-1} (= 100.1 × 0.193^2 kJ mol^{-1}). These deformation energies are produced by the steric interaction between the substituents and the macrocycle.

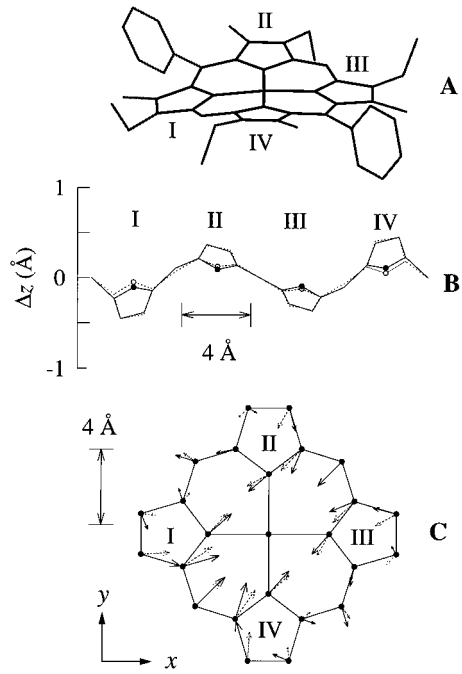

Figure 3. X-ray crystal structure of the strongly asymmetrically substituted nickel(II) 5,15-diphenyl-2,8,12,18-tetraethyl-3,7,13,17-tetramethylporphyrin (ref 24) [Ni(dPTETMP)] (panel A). The observed and simulated out-of-plane and in-plane distortions are displayed in solid lines and dotted lines, respectively. The out-of-plane distortion is illustrated by a linear display of the displacements of the 24 atoms with respect to the mean plane (panel B). The in-plane distortion, enlarged by a factor of 15, is shown by the individual displacement with respect to the reference structure (panel C). In the simulation, only the minimal basis is used.

TABLE 2: Out-of-Plane and In-Plane Displacements (Å) of the Minimal Basis for the X-ray Crystal Structures of Selected Metalloporphyrins. The Observed and Simulated Total Distortions D_{obs}^{oop}, D_{ibs}^{ip}, $D_{sim,1}^{oop}$, $D_{sim,1}^{ip}$ (Å) and the Mean Deviations $\bar{\delta}_{oop,1}$ and $\bar{\delta}_{ip,1}$ (Å) Are Also Listed[a]

	out-of-plane displacements (minimal basis)									in-plane displacements (minimal basis)								
porphyrin	D_{obs}^{oop}	$D_{sim,1}^{oop}$	$\bar{\delta}_{oop,1}$	*sad*	*ruf*	*dom*	*wav(x)*	*wav(y)*	*pro*	D_{obs}^{ip}	$D_{sim,1}^{ip}$	$\bar{\delta}_{ip,1}$	*m-str*	*N-str*	*trn(x)*	*trn(y)*	*bre*	*rot*
Ni(P)[b]	0.094	0.088	0.006	0.012	0.080	0.006	0.003	−0.033	−0.003	0.164	0.158	0.008	0.007	0.010	−0.004	−0.006	−0.157	0.000
Ni(OEP)/tri *A*[c]	0.087	0.078	0.007	0.000	0.000	0.000	0.030	−0.072	0.000	0.130	0.114	0.011	0.005	0.000	0.000	0.000	−0.114	−0.008
Ni(OEP)/tri *B*[d]	0.144	0.135	0.009	0.000	0.000	0.000	−0.066	0.117	0.000	0.148	0.128	0.014	0.005	−0.004	0.000	0.000	−0.127	0.008
Ni(OEP)/tet *C*[e]	1.461	1.461	0.003	0.115	1.456	0.000	0.000	0.000	0.000	0.330	0.291	0.027	0.000	0.000	0.000	0.000	−0.291	−0.008
Ni(TiPrP)[f]	1.811	1.804	0.029	−0.002	1.804	0.000	0.011	0.000	0.000	0.525	0.499	0.028	0.000	0.000	0.000	0.005	−0.499	0.000
Ni(TPP)[g]	1.321	1.317	0.017	−0.237	1.296	0.000	0.000	0.000	0.000	0.322	0.312	0.015	0.000	0.000	0.000	0.000	−0.311	−0.027
Cu(TPP)[g]	1.204	1.197	0.019	−0.183	1.183	0.000	0.000	0.000	0.000	0.192	0.165	0.019	0.000	0.000	0.000	0.000	−0.164	−0.020
Ni(TMP)[h]	0.314	0.301	0.015	0.077	0.147	−0.011	0.241	−0.066	0.016	0.169	0.140	0.017	−0.004	0.012	−0.007	0.012	−0.138	−0.013
Ni(OETPP)[i]	3.817	3.811	0.032	3.809	−0.092	−0.055	0.019	−0.060	0.009	1.147	1.039	0.097	−0.023	−0.053	−0.011	−0.038	−1.036	0.018
Ni(dPP)[j]	0.745	0.744	0.007	−0.075	0.736	0.059	−0.004	−0.048	0.007	0.219	0.205	0.013	−0.099	−0.004	−0.020	−0.010	−0.178	0.000
Ni(dtBuP)[k]	2.249	2.239	0.033	−0.021	2.182	0.488	−0.079	0.078	0.007	0.721	0.646	0.058	−0.261	−0.002	0.036	−0.043	−0.588	0.000
Cu(HETMP)[l]	1.741	1.732	0.027	−0.182	1.692	0.293	−0.137	0.028	−0.024	0.380	0.301	0.042	−0.207	−0.038	−0.006	−0.049	−0.209	0.000
Ni(dPTETMP)[m]	1.219	1.211	0.023	−1.192	0.000	0.000	0.154	0.154	0.000	0.295	0.264	0.024	−0.193	0.000	0.034	−0.034	−0.173	0.000
Tl(CN)(TPP)[n]	0.497	0.482	0.019	0.129	−0.042	0.458	0.047	−0.037	0.017	0.299	0.286	0.015	0.006	−0.050	−0.002	0.010	0.281	−0.010
Zn(py)(TNPCP)[o]	0.710	0.690	0.025	0.126	0.041	0.669	0.086	−0.057	0.008	0.156	0.129	0.016	0.000	0.035	0.023	−0.005	0.122	−0.003
$Fe(py)_2(TPP)$[p]	0.828	0.825	0.012	−0.430	0.697	0.060	−0.040	0.069	0.000	0.098	0.072	0.012	−0.010	0.000	0.000	−0.004	−0.071	0.000
Co(Cl)(Aq)(TPP)[q]	1.546	1.542	0.019	0.736	1.351	−0.084	0.042	−0.033	−0.011	0.319	0.285	0.025	0.024	−0.021	−0.026	0.022	−0.279	0.034
PH_2[r]	0.104	0.094	0.008	0.014	−0.088	−0.027	−0.016	0.004	−0.002	0.182	0.160	0.016	0.003	−0.012	0.007	0.007	0.159	0.002
$OEPH_2$[s]	0.126	0.109	0.011	0.000	0.000	0.000	0.089	0.063	0.000	0.250	0.229	0.018	0.000	0.057	0.000	0.000	0.221	0.000
$DPPH_2$-F_{28}[t]	0.660	0.650	0.021	0.000	0.000	0.000	0.613	0.215	0.000	0.335	0.329	0.011	−0.111	−0.118	0.000	0.000	0.286	0.000
Zn(P)/top	0.120	0.097	0.010	−0.026	−0.030	−0.065	0.059	−0.013	−0.003	0.140	0.136	0.006	0.014	−0.016	0.000	0.010	0.134	−0.003
Zn(P)/middle[u]	0.218	0.148	0.025	0.000	0.000	0.000	0.148	0.000	0.000	0.128	0.123	0.007	0.007	0.029	0.000	0.000	0.119	0.000
Zn(P)/bottom	0.120	0.097	0.010	0.026	0.030	0.065	0.059	−0.013	0.003	0.140	0.136	0.006	0.014	−0.016	0.000	−0.010	0.134	−0.003

[a] Displacements were obtained by orienting the macrocycle with its peripheral substituents according to Figure S1, that is, [Sb1Sb2]...Sm1...[Sb3Sb4]...Sm2...[Sb5Sb6]...Sm3...[Sb7Sb8]...Sm4. Location of the substituents and axial ligands with respect to the mean plane is indicated by a "+" (above) and a "−" sign (below). [b] Reference 26b. [c] [Et(+)Et(+)]...H...[Et(−)Et(−)]...H...[Et(−)Et(−)]...H...[Et(+)Et(+)]...H (ref 37). [d] [Et(+)Et(+)]...H...[Et(+)Et(−)]...H...[Et(−)Et(−)]...H...[Et(−)Et(+)]...H (ref 38). [e] [Et(+)Et(+)]...H...[Et(−)Et(−)]...H...[Et(+)Et(+)]...H...[Et(−)Et(−)]...H (ref 32). [f] [HH]...iPr(+)...[HH]...iPr(−)...[HH]...iPr(+)...[HH]... iPr(−) (ref 35). [g] [HH]...Ph(+)...[HH]...Ph(−)...[HH]...Ph(+)...[HH]...Ph(−) (refs 34b, 33). [h] [HH]...Me(+)...[HH]...Me(−)...[HH]...Me(−)...[HH]...Me(−) (ref 39). [i] [Et(+)Et(+)]...Ph...[Et(−)Et(−)]...Ph...[Et(+)Et(+)]...Ph...[Et(−)Et(−)]...Ph (ref 36). [j] [HH]...Ph(+)...[HH]...H...[HH]...Ph(+)...[HH]...H (ref 40). [k] [HH]...tBu(+)...[HH]...H...[HH]...tBu(+)...[HH]...H (ref 13). [l] [MeEt(−)]...Et(+)...[Et(−)Me]...H...[Me Et(−)]...Et(+)...[Et(+)Me]...H (ref 41). [m] [Et(+)Me]...Ph(+)...[MeEt(−)]...H...[Et(+)Me]...Ph(−)...[MeEt(−)]...H (ref 24). [n] [HH]...Ph(−)...[HH]...Ph(−)...[HH]...Ph(−)...[HH]...Ph(−), cyanide(+) (ref 42). The metal is about 0.910 Å displaced from the mean plane. [o] TNPCP is the abbreviation for *meso*-tetranitrophenylchiroporphyrin, αααα conformation, substituents (+). Pyridyl carbons of the axial ligand (+) are pointed in the direction of N1 and N3, pyridyl plane is slightly more tilted in the direction of N3 (ref 43). [p] [HH]...Ph(+)...[HH]...Ph(−)...[HH]...Ph(+)...[HH]...Ph(−). The pyridyl carbons (+) above the mean plane are oriented toward Cm2 and Cm4, whereas the pyridyl carbons (−) below the mean plane are pointed in the direction of Cm1 and Cm3 (ref 44). [q] [HH]...Ph(+)...[HH]...Ph(−)...[HH]...Ph(+)...[HH]...Ph(−), chlorine(+), water molecule (−) (ref 45). [r] Protons on the pyrrole nitrogen atoms are located in *x* direction (ref 46). [s] [Et(+)Et(+)]...H...[Et(+)Et(+)]...H...[Et(−)Et(−)]...H...[Et(−)Et(−)]...H. Protons on the pyrrole nitrogen atoms are located in *x* direction (ref 47). [t] [Ph(−)Ph(−)]...Ph...[PhPh]...Ph...[Ph(+)Ph(+)]...Ph...[PhPh]...Ph (ref 48). [u] Deviation between the observed and simulated nonplanar total distortion is due to localized perturbations. By using the extended basis, the total simulated distortion is 0.216 Å and the displacements are for $d_1^{Eg(x)} = 0.154$ Å and $d_2^{Eg(x)} = 0.157$ Å (ref 26a). Also, notice that the displacement $d_1^{Eg(x)}$ obtained with the minimal basis (0.148 Å) is almost unchanged from that obtained with the extended basis (0.154 Å); this is a consequence of the near orthogonality of $\hat{\mathbf{D}}_1^{Eg(x)}$ and $\hat{\mathbf{D}}_2^{Eg(x)}$.

The most commonly observed symmetric out-of-plane distortions are *sad* (B_{2g}) and *ruf* (B_{1g}) deformations. For example, the crystal structure of the tetragonal form of Ni(OEP)[32] exhibits the *ruf* deformation. The *ruf* deformation is also often seen for the crystal structures of metal *meso*-tetraphenylporphyrins such as Cu(TPP)[33] and the recently obtained crystal structure of Ni(TPP).[34b] For Ni(TPP), planar and nonplanar conformations coexist in solution due to the effect of the small nickel ion,[34a] but crystallization apparently selects out the *ruf* species. In fact, the *ruf* deformation of most metal *meso*-tetraphenylporphyrins is probably due to the effect of crystal packing forces on the orientation of the phenyl groups. As a result, the solution structures may be expected to differ from the crystal structures. The reasons for the frequent appearance of the *ruf* deformation are the very low force constant (frequency) of the mode ($K_1^{B1u} = 16.5$ kJ mol^{-1} Å^{-2}) and the high effectiveness of this deformation in relieving steric strain for many substituted porphyrins.

The interactions of substituents with the macrocycle are generally symmetric when the porphyrin is symmetrically substituted. The distortion observed is frequently also symmetric, that is, the distortion occurs along only a few of the normal deformations. The orientations of the substituents also play a significant role in determining the symmetry of the perturbation on the macrocycle. As an example, we reported recently that nickel(II) *meso*-tetraalkylporphyrins give the *ruf* deformation as the lowest-energy conformation in the energy-minimized calculations,[7] and this is confirmed by several X-ray crystal structures including nickel(II) *meso*-tetra-*iso*-propylporphyrin [Ni(TiPrP)].[35] The *ruf* deformation results from an $\alpha\beta\alpha\beta$ orientation of the alkyl substituents relative to the mean plane. Other orientations give higher-energy conformers. In particular, the $\alpha\alpha\alpha\alpha$ orientation of the substituents gives a purely *dom* deformation and the $\alpha\alpha\beta\beta$ orientation gives a pure *wav*(x) deformation. The degree of these distortions depends on the size of the substituents.

Sterically bulky substituents are able to lock in a strongly nonplanar X-ray crystal structure even in solution. For example, metal octaethyltetraphenylporphyrins show large *sad* deformations in crystal structures of Ni(OETPP)[36] and Cu(OETPP).[21a] The magnitudes of the out-of-plane and in-plane distortions of Ni(OETPP) are the largest found so far (Table 2). Nevertheless, even in this case the match between the observed and simulated distortions using the minimal basis is good, but the second lowest-frequency normal coordinates are required to simulate the distortion more accurately. This finding is not surprising given the large energy involved in this macrocyclic distortion.

If the substituents and the crystal packing forces lower the symmetry enough, more than one out-of-plane normal deformation is required. Examples in Table 2 are Ni(P),[26b] the triclinic forms of Ni(OEP),[37,38] and Ni(TMP) (*meso*-tetramethylporphyrin).[39] The recently crystallized structure of Ni(P) is almost planar; however, closer examination of the macrocycle shows small but significant contributions from *ruf* and *wav*(y) deformations induced by packing forces. The nearly planar crystal structures of Ni(OEP) also exhibit both the *wav*(x) and *wav*(y) deformations. Moreover, a crystal structure of Ni(TMP)[39] is significantly nonplanar; its nonplanar distortion is largely a combination of *ruf* and *wav*(x) with smaller contributions of *sad* and *wav*(y) deformations. For Ni(OEP) and Ni(TMP), both the crystal packing and the substituents probably account for the distortions.

For substituted porphyrins for which the substituent pattern reduces the symmetry from D_{4h} for the ideal planar porphyrin, the displacements occur along several or all lowest-frequency normal coordinates. Still, the *sad*, *ruf*, *dom* (out-of-plane) and *m-str*, *N-str*, *trn* (in-plane) deformations are energetically favored to relieve steric strain most efficiently. Consequently, their displacements will often be the largest. For example, the crystal structures of 5,15-disubstituted porphyrins like Ni(dPP)[40] (5,15-diphenylporphyrin) and Ni(dtBuP)[13] (5,15-di-*tert*-butylporphyrin) are mostly ruffled. Also, as expected, the *m-str* (B_{2g}) in-plane deformation is present. Moreover, in the case of the highly asymmetric substitutions of Cu(HETMP)[41] and Ni(dPTETMP),[24] normal deformations of all symmetry types can contribute. The in-plane *bre* deformation (A_{1g}) depends on the metal in the reference structure. For copper porphyrins most of the *bre* deformation results from other perturbations on the structure, but for nickel porphyrins about -0.1 Å of the *bre* deformation results from replacement of copper (the reference metal) with nickel. The rest is due to other perturbations on the macrocyclic structure (Table 2).

Another frequently encountered type of porphyrin distortion is caused by axial coordination. In the five-coordinate complexes, the axial ligand often causes a displacement of the metal out of the mean plane. The resulting nonplanar distortion of the macrocycle is typically a *dom* deformation, usually accompanied with the in-plane *bre* deformation. This also often occurs in six-coordinated complexes with different axial ligands. Porphyrins with very large metal ions also favor the *dom* deformation type. Good examples of the *dom* deformation are Tl(CN)(TPP)[42] and $\alpha\alpha\alpha\alpha\alpha$ Zn(py)(TNPCP)[43] (*meso*-tetranitrophenylchiroporphyrin) listed in Table 2. Finally, the structures of a number of six-coordinated complexes with the same or different axial ligands, such as Fe(py)$_2$(TPP)[44] and Co(Cl)(H$_2$O)(TPP),[45] crystallize in *ruf* and *sad* deformation types with relatively small *dom* contributions.

Although the minimal basis is strictly not applicable for the crystal structures of free-base porphyrins, we have analyzed the crystal structures of PH_2,[46] $OEPH_2$,[47] and $DPPH_2$-F_{28} (fluorinated dodecaphenylporphyrin[48]). The decomposition results are listed in Table 2. Surprisingly, the deviations $\bar{\delta}_1$ between the observed and simulated distortions are relatively small, thus providing evidence that the minimal basis may also be used for the crystal structures of free-base porphyrins. Interestingly, both crystal structures of $OEPH_2$ and $DPPH_2$-F_{28} exhibit only the *wav* deformations. In particular, the structure of $DPPH_2$-F_{28} exhibits the largest *wav* deformation found so far. The rarity of large *wav* deformations for metalloporphyrins confirms that a large energy is required to induce this type of deformation. The reason for the more common occurrence of the *wav* deformations for the free-base porphyrins is probably associated with the E_g symmetry of the perturbation induced by opposing protons in the porphyrin core, one above and one below the mean plane. Alternatively, the corresponding vibrational normal-mode frequency might be considerably lower for free-base porphyrins.

Limits of Using the Minimal Basis. The total observed distortions, D_{obs}^{oop} and D_{obs}^{ip}, the total distortions simulated by using the displacements along the lowest-frequency modes (minimal basis), $D_{sim,1}^{oop}$ and $D_{sim,1}^{ip}$, and the mean deviations, $\bar{\delta}_{oop,1}$ and $\bar{\delta}_{ip,1}$, between the observed and simulated distortions are listed in Table 2. The mean deviations given by eq 17 can be compared to the error estimates of the position of a single atom in X-ray crystallography. Assuming that the utmost care is taken as to diffractometer alignment, absorption and extinction correction, and crystal quality, the *maximum error* remaining in the best diffraction experiment can cause uncertainties as large as 0.006 Å in atomic distances for small molecules.[49,50] Of

course, when the normal-deformation basis set is truncated to only the minimal basis, we expect larger deviations between the observed and simulated structures. However, the minimal-basis decomposition of more than 100 X-ray crystal structures reveals that the mean deviations $\bar{\delta}_{oop,1}$ or $\bar{\delta}_{ip,1}$ are typically in the range 0.003−0.030 Å. Thus, many of the structures require the extended basis for the simulated structure to agree with the observed structure to within the experimental error. However, a few structures, Ni(OETPP),[36] Ni(dtBuP),[13] and Cu(HETMP)[41] (see Table 2), exhibit large deviations between the observed and simulated distortions. Significantly, when simulated using the normal deformations of the extended basis, the structures obtained are greatly improved. These few structures are examples for which steric crowding of substituents give rise to large distortion energy, resulting in the occupation of higher-frequency normal coordinates ($\hat{\mathbf{D}}_m^{\Gamma}$, $m > 1$).

According to eq 18, the probability that a significant normal deformation $\hat{\mathbf{D}}_m^{\Gamma}$ ($m > 1$) occurs in addition to $\hat{\mathbf{D}}_1^{\Gamma}$ is energetically proportional to the square of the frequency ratio $(\tilde{\nu}_1^{\Gamma}/\tilde{\nu}_m^{\Gamma})^2$. In other words, the extended basis is most often necessary for deformations for which the frequency ratio $(\tilde{\nu}_1^{\Gamma}/\tilde{\nu}_2^{\Gamma})^2$ is close to 1 (Table 1). On this basis, the presence of E_g and E_u deformation types may produce significant deviations between the observed and simulated distortions for the minimal basis. On the other hand, large B_{2u} and B_{1u} deformation types occur almost purely along their corresponding lowest-frequency normal coordinates, partly because their frequency ratios are small. Moreover, larger deviations between the observed and simulated structure by using the minimal basis are more likely to be encountered for the in-plane than for the out-of-plane distortions because (1) the frequency ratios are generally closer to unity and (2) the degree of freedom is essentially higher for the in-plane than for the out-of-plane distortions. For very large distortions, these are the factors to be considered.

In the normal-mode calculation, the secular equations are solved by assuming small oscillations about the local minimum. Very large distortions, however, violate this assumption and intermixing of modes or even the appearance of new types of modes may occur. Nonetheless, the largest out-of-plane distortion found so far is for Ni(OETPP),[36] and it can be described reasonably by using only the lowest-frequency normal modes. Finally, perturbations localized at a single atom or small groups of atoms also induce distortions that require, of course, the extended or even larger basis sets for an accurate description. An example is the structure of the recently crystallized trimer of Zn(P).[26a,51]

To sum up, we find that the macrocycles of numerous crystal structures of synthetic metalloporphyrins are adequately classified and quantified in terms of the lowest-frequency normal coordinates (minimal basis). However, large or highly energetic distortions and localized perturbations require the extended basis or even normal deformations $\hat{\mathbf{D}}_m^{\Gamma}$ with $m > 2$. In this case, the use of the total deformations of each symmetry type (eq 8) for characterizing these distortions is recommended.

Structural Decomposition of X-ray Crystal Structures of Protein-Bound Porphyrins. The structural decomposition method has also been used to analyze the heme distortions in more than 150 hemoprotein X-ray crystal structures. The asymmetric environment of the heme group in a protein induces simultaneous displacements along several or all of the lowest-frequency normal coordinates, making the distortion difficult to characterize by eye. The structural decomposition method, however, projects out the contribution of each symmetric deformation type to the total distortion, providing a simple and sensitive measure of these complicated structures. The method also furnishes an important new probe of the protein environment of the heme group that, in some cases, reveals previously hidden influences of the protein on the active site.[52]

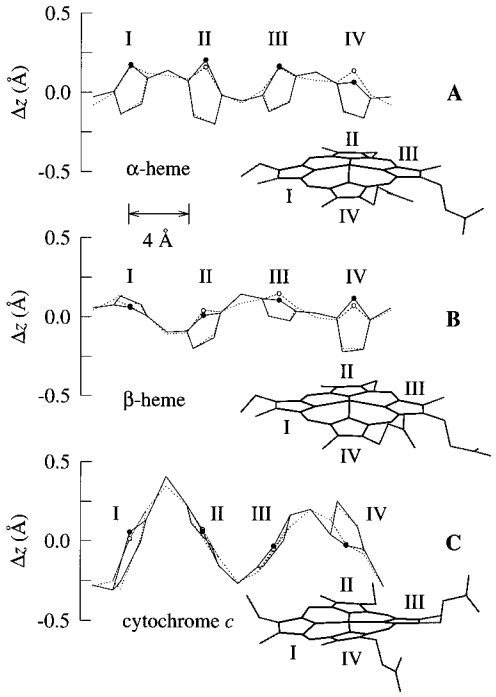

Figure 4. X-ray crystal structures (ref 54) of the heme groups (C and D from ref 54a, 2HHB) of the α- and *β*-chains of human deoxyhemoglobin (panels A and B) and cytochrome *c* (ref 58a, 1YCC) (panel C). The out-of-plane distortion is illustrated by a linear display of the observed (solid lines) and simulated (dotted lines) displacements of the 24 atoms with respect to the mean plane. In the simulation, only the minimal basis is used.

Since the biologically relevant iron porphyrins are expected to be nearly planar in solution, it must be the multitude of interactions with amino acids lining the heme pocket that locks the porphyrin into its nonplanar geometry. Although the environment is composed of many localized contacts, the structures of the heme groups in the proteins from different biological systems are found to be adequately described by using only the lowest-frequency normal coordinates (minimal basis).[52] This suggests that the localized perturbations are probably weak individually, but collectively give rise to the observed structure. Nevertheless, it has to be noted that the resolution of the protein X-ray crystal structures is much poorer than the X-ray crystal structures of small synthetic metalloporphyrins (minimum mean error of 0.030 Å for proteins[52] compared to about 0.003 Å for synthetic porphyrins[50]), making it difficult to rule out significant displacements along high-frequency modes. In the discussion that follows, we confine our attention to the out-of-plane distortions since in most cases the in-plane displacements are near the estimated upper limit of errors in the protein X-ray structures (≈0.10 Å at approximately 2.0-Å resolution[20,53]). The corresponding in-plane displacements are listed in Tables S14−S17 available in the Supporting Information.

Human Deoxyhemoglobin A. A revealing application of the method is the decomposition of the structures of the heme groups in the α- and *β*-chains of human deoxyhemoglobin A structures.[54] In Figure 4 (panels A and B), the out-of-plane displacements are illustrated for the heme groups of one α- and *β*-chain taken from a hemoglobin X-ray structure.[54a] Figure 5 displays the minimal-basis displacements of the heme groups of all of the human deoxyhemoglobin structures[55] contained in the Brookhaven Protein Data Bank (PDB).[56] (Table S14 in the Supporting Information lists the values of the out-of-plane and in-plane displacements.) Figure 5 also illustrates the mean values and standard deviations of the displacements. In all, there

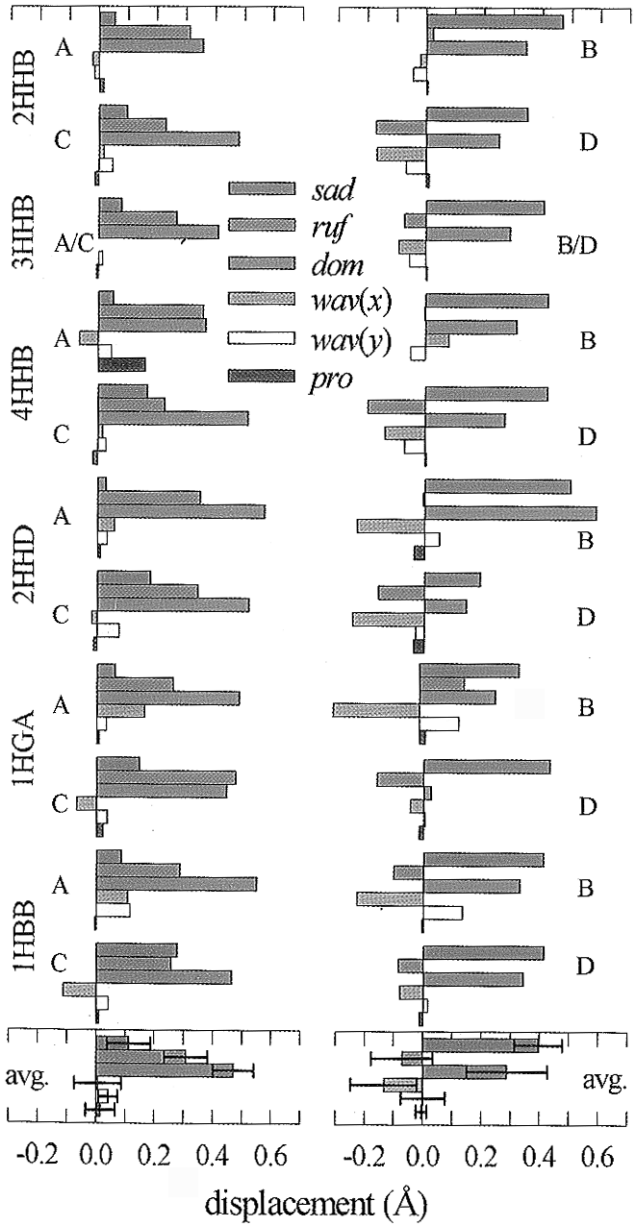

Figure 5. Out-of-plane displacements (minimal basis) for the four heme groups (A, B, C, D) in the human deoxyhemoglobin X-ray crystal structures (resolution ≤2.2 Å) obtained by using three different refinement methods and from four different working groups (ref 54). PDB reference codes (ref 56) are given. The in-plane displacements are tabulated in the Supporting Information. The orientation of the macrocycle and the location of the axial ligands in the simulation, the refinement methods, X-ray crystal structure resolution, and crystallization condition are given in ref 55.

are 11 α-chain and 11 β-chain heme groups taken from three independent X-ray structures. In the case of the structure by Fermi and co-workers (PDB reference codes 2HHB, 3HHB, 4HHB),[54a] three protein structures are given, each the product of a different method of refinement. The structure of Kavanaugh and co-workers (PDB reference code 1HBB)[54d] is obtained from a crystal grown under low-salt conditions. The mean deviation $\bar{\delta}_{oop,1}$ between the observed and simulated distortions is approximately 0.030 Å. The variation for different X-ray crystal structures in each of the displacements for a particular subunit is about 0.1 Å (see error bars for the average displacements in Figure 5). This value is similar to the errors in the coordinates of a single atom in protein X-ray crystallography.[20,53] Nonetheless, some of this variation could represent real differences of the heme groups between chains in the different crystals.

There are well-known structural and functional differences in the protein environments of the heme group in the α- and β-subunits of deoxyhemoglobin,[54a,d,57] for example, resulting in the heme groups of the α-chains having higher oxygen affinity than those of the β-chains.[57] Therefore, it was of interest to see whether the new method could uncover any unreported differences in the heme structures of the subunits. For the heme groups in the α-chains, examination of the displacements given in Figure 5 shows that these heme groups are primarily domed (0.5 Å), with an only slightly smaller contribution from ruffling (0.3 Å). A small *sad* contribution (0.1 Å) might also be present in the α-chains. All other deformations are statistically insignificant. In contrast, for the heme groups in the β-chains, the predominant deformation type is *sad* (0.4 Å), with less *dom* deformation (0.3 Å) than for the α-chains. A negative *wav*(*x*) (−0.1 Å) contribution may also be significant. The total distortion for both the α- and β-heme groups is 0.6 Å, and this is well simulated with just the minimal basis. Clearly, these systematic structural differences between the α- and β-heme groups are not artifacts of the X-ray refinement methods or of crystallization.

Yeast Ferrocytochrome c and its Mutants. The nonplanar distortion is most likely to be functionally significant when it is large. One case for which a large distortion is found is for the heme group of isozyme-1 ferrocytochrome *c*[58a] and its 16 mutants.[58b−g] In this case, it was also of interest to see whether the decomposition method can determine any structural differences between the heme group of the wild type and mutants. Earlier, we noted no clear differences in the heme structure for mitochondrial cytochrome *c* from different species for which there is natural variation in the amino acid sequence.[59]

In Figure 4 (panel C), the linear display of the simulated structures of the wild-type isozyme-1 ferrocytochrome *c* for the minimal basis is illustrated along with the X-ray crystal structure.[61] The total observed and simulated distortion is 0.9 Å, and the mean deviation $\bar{\delta}_{oop,1}$ between the observed and simulated distortion is 0.032 Å. From the decomposition results in Figure 6, it can be seen that the macrocycle is mainly ruffled (0.8 Å) as noted by other authors.[9,58a,62,63] However, a negative *sad* deformation (−0.3 Å) is also present. Small, almost equal amounts of *wav*(*x*) and *wav*(*y*) deformations (0.2 Å) are also significant.

The effect of equal *wav*(*x*) and *wav*(*y*) deformations alone is to raise one *meso* carbon above the mean plane and equally lower the opposite one, leaving the other *meso* carbons in the plane. This distortion is best illustrated by the αβ conformer of the 5,15-disubstituted porphyrins.[13] A ruffling alone leaves opposite carbon atoms equally displaced and alternatively above and below from the mean plane. Together the *ruf* and *wav*(*x*) + *wav*(*y*) deformations give a distortion in which one *meso* carbon is highly displaced from the mean plane, the two adjacent *meso* carbons are displaced on the opposite side of the mean plane but have small displacements, and the opposite *meso* carbon is displaced on the same side with the smallest displacement from the plane. Examination of Figure 4 (panel C) shows that the *meso* carbon atom between pyrroles I and II, which have the covalent thioether bonds to the protein, is much more displaced than the other *meso* carbons. Obviously, pyrroles I and II are more tilted with respect to the mean plane than are pyrroles III and IV.[58a,62] The latter pyrroles are more weakly linked to the protein via the hydrogen bonds of the propionate groups. Thus, the thioether bonds appear to shorten the distance between pyrrole rings I and II, causing them to buckle and resulting in the large displacement of the *meso* carbon atom between them. This appears in the decomposition besides the *ruf* deformation as the *wav*(*x*) + *wav*(*y*) deformation.

Figure 6 illustrates the decomposition results for the X-ray

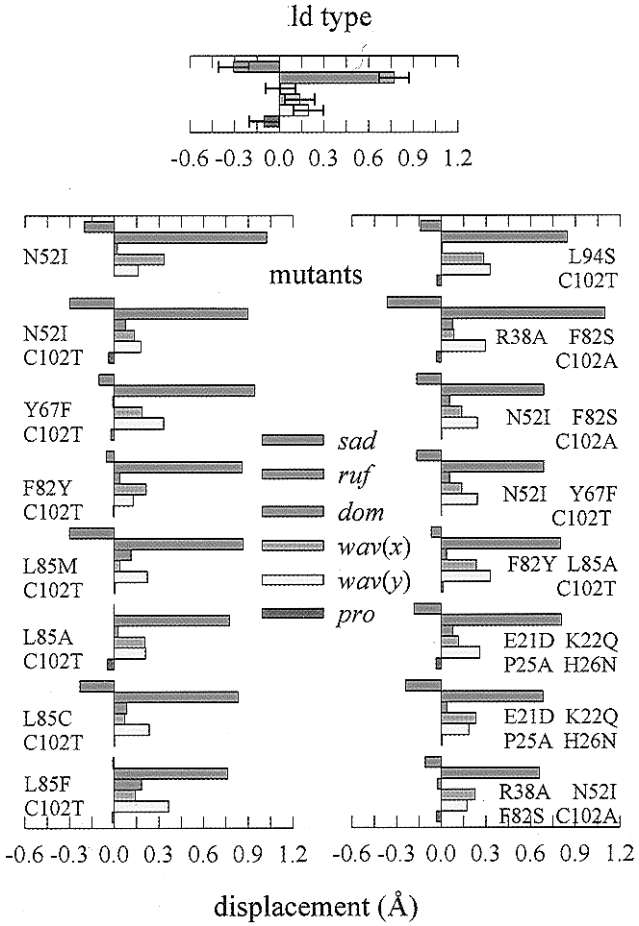

Figure 6. Out-of-plane displacements (minimal basis) for the heme group in the X-ray crystal structures of yeast isozyme-1 ferrocytochrome *c* (resolution ≤2.1 Å) of the wild type (ref 58a) and mutants (ref 58b−g). The in-plane displacements are tabulated in the Supporting Information. One-letter symbols are used for the amino acid replacements (ref 60). The orientation of the macrocycle and the location of the axial ligands in the simulation as well as the X-ray crystal structure resolution are given in ref 61.

TABLE 3: Characterization of the Amino Acid Residues Replaced in the Mutants of Yeast Isozyme-1 Cytochrome *c* (*Saccharomyces cerevisiae*)[a]

	21[b]	22	25	26	38	52	67	82	85	94	102
	E[c]	K	P	H	R	N	Y	F	L	L	C
aromatic							●	●			
heme-contact							●		●	●	
interior						●	●		●	●	●
conserved	●				●		●	●		●	

[a] Residues were characterized according to ref 59. One-letter symbols are used for the amino acids (ref 60). [b] This horizontal row of numbers refers to the amino acid number. [c] This horizontal row of letters refers to the wild type.

crystal structures of the heme groups of the yeast ferrocytochrome *c* mutants; the displacements for the wild type and the approximate errors are also shown. (Table S15 in the Supporting Information lists the values of the out-of-plane and in-plane displacements.) The decomposition of the heme structures of 16 mutants[58b−g] includes the crystal structures of one mutant with a single mutation, eight mutants with double mutations, three mutants with triple mutations, and four mutants with quadruple replacements. The amino acid mutations are characterized into aromatic, heme-contact, interior, and conserved categories summarized in Table 3. In this context, conserved residue means that the amino acid is maintained for all species.

The total distortion varies among the mutants from 0.7 and 1.2 Å, a possibly significant variation. However, distribution among the normal deformations suggests that the replacements have only a small influence on the heme structure. Even the replacement of tyrosine-67, which is known to alter the local heme environment[58c] and is a heme-contact and conserved residue, has only minor influence on the heme distortion. Hence, the heme structure appears to be highly constant even when heme-contact and conserved amino acids are altered. This fact, together with the lack of significant species variation, strongly suggests that the cause of the heme distortion in *c*-type cytochromes is localized in a small segment of the protein.

These results support the hypothesis that the distortion of the heme group results from the covalently linked segment (Cys−Leu−Gln−Cys−His segment shown in Figure 7). If this peptide segment is the source of the distortion energy responsible for the nonplanar conformation, then deleting or modifying residues in this segment should cause a significant change in the heme conformation.

Cytochromes c_3. The hypothesis that the protein segment is a major factor in causing the heme distortion is substantiated by the decomposition results for the crystal structures[65,66] of the four-heme cytochromes c_3. Figure 8 gives the deformations for each of the four hemes of cytochrome c_3. (Heme numbering scheme is based on the appearance of the heme-binding cysteine residues in the primary sequence.) The decomposition results are given for four strains, including two from *D. vulgaris* (Hildenborough[65a] and Miyazaki[65b]) and two from *D. sulfuricans* (ATCC 27774[65c] and Norway[65d]). (Table S16 in the Supporting Information gives the values of the out-of-plane and in-plane displacements of each heme group.[67]) The amino acid sequence of the covalently linked peptide segment of each heme group is summarized in Table 4. All the fifth and sixth axial ligands to the heme irons are histidines. In a single protein, the distortions of the four hemes vary remarkably. For example, heme 1 is mainly ruffled, whereas heme 4 is mostly saddled. The different number and types of residues between the cysteines for each heme (see Table 4) account for this observation. Further, the peculiarity of the structure of heme 4 of Norway relative to the other strains provides additional evidence for this conclusion. A unique deletion of two of the four residues in this peptide segment for Norway accounts for its structural peculiarity and causes the different distortions of heme 4.

While the distortions are clearly different for the four hemes in a single protein, among different strains, corresponding hemes have remarkably similar heme conformations. For example, in all four strains heme 1 is primarily ruffled. This is a surprising result because about 10 residues out of approximately 110, other than the 8 axial histidines and 8 covalently bound cysteines, are conserved for the four strains. In spite of this large variation in the amino acid sequence, the conformation of corresponding hemes is conserved, emphasizing the importance of the small covalently linked segment in causing the heme distortion.

Finally, molecular mechanics calculations on the heme−pentapeptide convincingly show that the heme group is nonplanar when the covalently linked peptide segment is intact, and almost planar in its absence.[68] Thus, the molecular mechanics calculations corroborate the hypothesis that the linkage Cys−X−Y−Cys−His is most likely the main source of the distortion energy.

Other Hemoproteins. Figure 9 illustrates the results of the out-of-plane decomposition of the X-ray crystal structures[69,70] of heme groups in a variety of proteins. (Table S17 in the Supporting Information gives the corresponding in-plane displacements.) The proteins in Figure 9 were chosen to show the large variation in types and magnitudes of out-of-plane

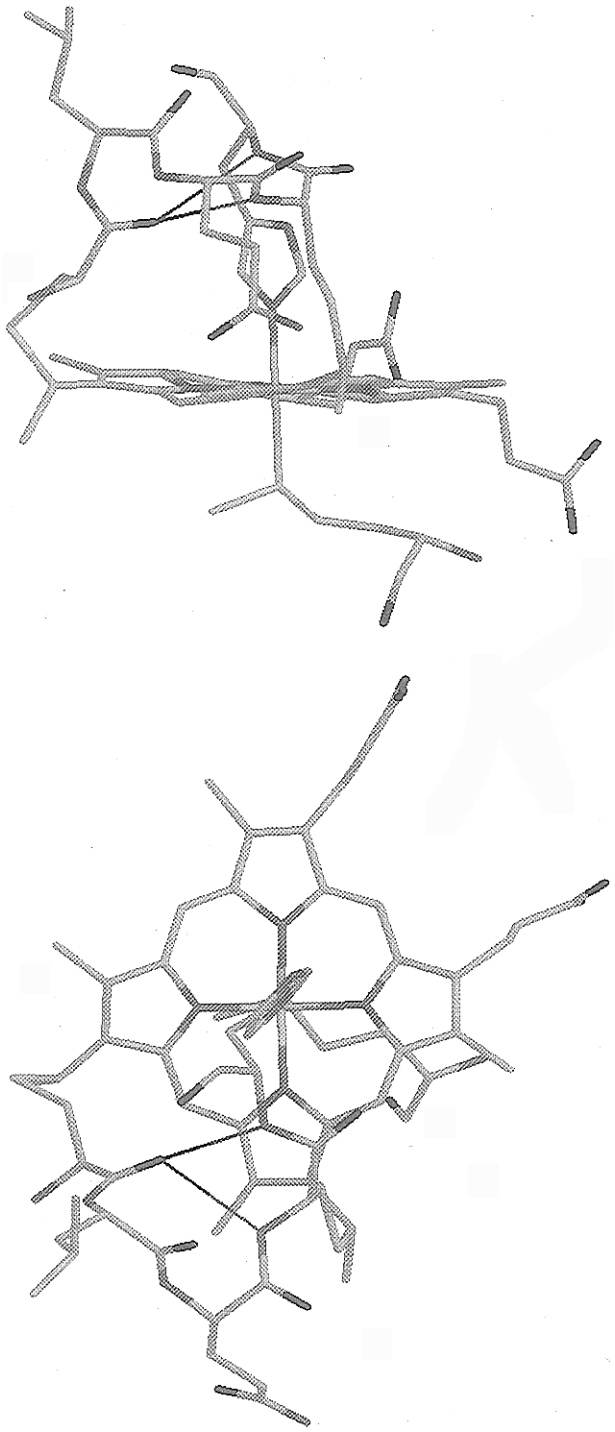

Figure 7. Edge-on and top view of the covalently linked peptide segment Cys−Leu−Gln−Cys−His of the heme group of yeast isozyme-1 ferrocytochrome in the X-ray crystal structure *c* (1.23-Å resolution, ref 58a). The hydrogen-bonding interactions in the backbone are indicated by lines. Figures were created with the molecular visualization program RasMol (ref 64).

distortions[71] that occur for proteins with different biological functions. As for the mitochondrial cytochromes *c*, many of the distortions are conserved within a functional class.[52] Hence, the structural decomposition method provides a useful tool for systematic exploration of the role of distortions of tetrapyrroles in biochemical mechanisms.

Conclusions

The X-ray crystal structures of synthetic metalloporphyrins and heme groups contained in proteins have been analyzed successfully using a new structural decomposition method for

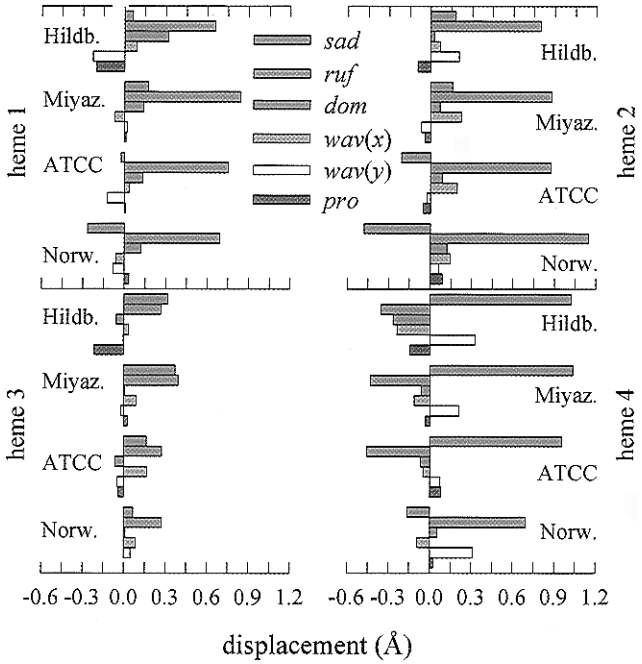

Figure 8. Out-of-plane displacements (minimal basis) for the four heme groups in the X-ray crystal structures of cytochromes c_3 from *D. vulgaris* [Hildenborough (ref 65a) and Miyazaki (ref 65b)] and *D. sulfuricans* [ATCC 27774 (ref 65c) and Norway (ref 65d)]. The in-plane displacements are tabulated in the Supporting Information. The heme numbering is based on the amino acid sequence (see footnote of Table 4). The orientation of the macrocycle in the simulation and X-ray crystal structure resolution are given in ref 66.

TABLE 4: Covalently Linked Peptide Segments of the Four Heme Groups in Cytochrome c_3 from *Desulfovibrio vulgaris* (Hildenborough and Miyazaki) and *D. sulfuricans* (ATCC 27774 and Norway). All the Fifth and Sixth Axial Ligands to the Heme Irons are Histidine Nitrogen Atoms[a]

heme[b]	Hildenborough	Miyazaki	ATCC	Norway
heme 1	C**GD**--C	C**GD**--C	C**VT**--C	C**VQ**--C
heme 2	C**GTAG**C	C**ATAG**C	C**GSSG**C	C**TTSG**C
heme 3	C**VG**--C	C**VG**--C	C**LA**--C	C**ID**--C
heme 4	C**KKSK**C	C**KGSK**C	C**AKSK**C	C-**G**-**K**C

[a] One-letter symbols are used for the amino acids (ref 60). [b] Heme numbering scheme is based on the appearance of the heme-binding cysteine residues in the primary sequence, *i.e.*, heme 1 is the first covalently bound heme. Hildenborough (ref 65a), Miyazaki (ref 65b), ATCC (ref 65c), Norway (ref 65d).

classifying and quantifying their out-of-plane and in-plane distortions. In most cases, the analysis shows that the macrocyclic displacements can be described properly by using only the lowest-frequency normal coordinates of the macrocycle because they require the least energy to overcome interactions resulting, for example, from bulky substituents at the porphyrin periphery. The method provides a unique way of characterizing the distortions of the macrocycle. As can be seen from Table 1, the in-plane distortions demand considerably more energy; therefore, their displacements are much smaller than the out-of-plane ones. For the structures examined in this work, the in-plane deformations are only statistically significant for the high-resolution X-ray crystal structures.

The structural decomposition method is particularly helpful when applied to the complicated distortions of the heme groups in proteins. Moreover, it provides an important new probe of the protein environment of the heme active site and, in some cases, reveals previously hidden influences of the protein on the heme conformation. In the case of *c*-type cytochromes, analysis of the influence of natural sequence variation and engineered mutations suggests that the source of the heme

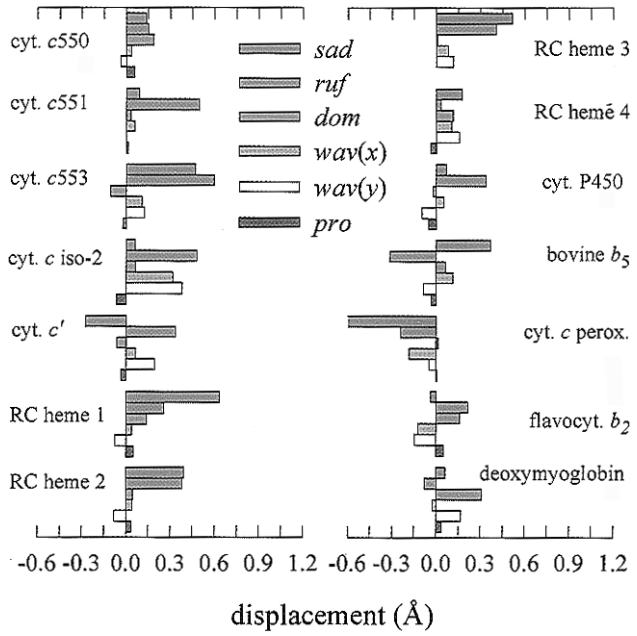

Figure 9. Out-of-plane displacements (minimal basis) for the heme groups in the X-ray crystal structures of selected hemoproteins (ref 69). The in-plane displacements are tabulated in the Supporting Information. The orientation of the macrocycle and the location of the axial ligands in the simulation, the X-ray crystal structure resolution, and the PDB reference codes are given in ref 70.

distortion is most likely concentrated in a small segment of the protein, the covalently linked peptide segment. The heme structures and their conformational changes are thought to be possible mechanisms for protein modulation of the biological properties of tetrapyrroles. However, the electronic effects of axial ligands, the multitude of interactions of nearby amino acid residues, and the hydrogen bonds are probably similarly important.

Unfortunately, direct relationships between the heme structure and its biological function are still not confirmed; however, the normal structural decomposition method provides the needed framework for systematic exploration of the role of distortions of tetrapyrroles in biochemical mechanisms. Moreover, the method has already revealed successfully a variety of relationships between the structure of the protein surrounding the heme group and its out-of-plane distortions.[52] The structural decomposition method also makes possible the discovery of correlations between spectral properties and specific types of normal deformations of model metalloporphyrins. In the future, these structural and spectral correlations should aid in the search for relationships between heme structure and function.

Acknowledgment. This work was supported by the United States Department of Energy under Contract DE-AC04-94DP85000 (J.A.S.) and Associated Western Universities graduate (X.S.) and postdoctoral fellowships (W.J.). Sandia is a multiprogram laboratory operated by Sandia Corporation, a Lockheed Martin Company, for the United State Department of Energy. The authors greatly appreciate Drs. Mathias O. Senge (Freie Universität Berlin, Germany), Daniel J. Nurco (University of California, Davis), and Marinella Mazzanti (Laboratoire de Chimie de Coordination, Grenoble, France) for communicating their X-ray crystal structure of nickel(II) 5,15-diphenyl-2,8,12,18-tetraethyl-3,7,13,17-tetramethylporphyrin,[24] nickel(II) 5,15-diphenylporphyrin,[40] fluorinated dodecaphenylporphyrin,[48] and zinc(py) *meso*-tetranitrophenylchiroporphyrin[43] prior to publication.

Supporting Information Available: Appendix A, giving the mathematical procedure for removing the translational and rotational contributions. Appendix B, describing the determination of the mean plane and final *z*-axis rotation of the observed structure providing the basis for the calculation of the observed individual displacements of the macrocyclic atoms (*i.e.*, the vector $\mathbf{D}_{obs}$). Appendix C, giving the mean and root-mean-square deviation (or positional error) in different dimensions assuming a Gaussian-distributed probability density function. Appendix D, presenting the results of the normal-mode calculations on Ni(P) and symmetrically substituted porphyrins. Table S1, listing the normalized atomic displacement coordinates of the zero-frequency eigenvectors representing rigid body translation and rotation of the D_{4h}-symmetric porphyrin macrocycle. Table S2, listing the symmetry-adapted atomic coordinates of the X-ray crystal structures of Cu(P) along with Ni(P), Co(P), and Zn(P). Tables S3 and S4, giving the atomic displacement coordinates of the normal deformations $\hat{\mathbf{D}}_m^{\Gamma}$ and their corresponding calculated normal-mode frequencies. Only the corresponding three lowest-frequency out-of-plane and in-plane coordinates are listed. Table S5, giving the out-of-plane and in-plane displacements of the extended basis for the X-ray crystal structures of the synthetic metalloporphyrins listed in Table 2. Table S6, giving the lowest calculated and observed vibrational frequencies of the out-of-plane and in-plane normal modes of each symmetry for Ni(P). Tables S7−S13, listing the calculated frequencies and dot products s_{kj}^{Γ} of the three lowest-frequency out-of-plane and in-plane eigenvectors of the copper macrocycle and some selected copper porphyrins. Table S14, giving the out-of-plane and in-plane displacements (minimal basis) of the heme groups in the X-ray crystal structures of human deoxyhemoglobin A. Table S15, listing the out-of-plane and in-plane displacements (minimal basis) of the heme groups in the X-ray crystal structures of the wild type and mutants of yeast isozyme-1 ferrocytochrome *c*. Table S16, giving the out-of-plane and in-plane displacements (minimal basis) of the heme groups in the X-ray crystal structures of cytochrome c_3. Decomposition results of strains Hildenborough, Miyazaki, ATCC 27774, and Norway are listed. Table S17, listing the out-of-plane and in-plane displacements (minimal basis) of heme groups in the X-ray crystal structures of selected hemoproteins. Figure S1, showing the atomic labeling of the macrocyclic atoms and peripheral substituents. Figures S2 and S3, illustrating the out-of-plane and in-plane normal deformations $\hat{\mathbf{D}}_2^{\Gamma}$ and $\hat{\mathbf{D}}_3^{\Gamma}$. Figure S4, illustrating the bond angles and distances of the X-ray crystal and energy-minimized structure of Ni(P). Figure S5, showing the crystal packing arrangement of the trimer configuration of Zn(P) (76 pages). Ordering information is given on any current masthead page.

References and Notes

(1) (a) Kratky, C.; Waditschatka, R.; Angst, C.; Johansen, J.; Plaquevent, J. C.; Schreiber, J.; Eschenmoser, A. *Helv. Chim. Acta* **1982**, *68*, 1312. (b) Waditschatka, R.; Kratky, C.; Jaun, B.; Heinzer, J.; Eschenmoser, A. *J. Chem. Soc., Chem. Commun.* **1985**, 1604. (c) Geno, M. K.; Halpern, J. *J. Am. Chem. Soc.* **1987**, *109*, 1238. (c) Furenlid, L. R.; Renner, M. W.; Smith, K. M.; Fajer, J. *J. Am. Chem. Soc.* **1990**, *112*, 1634.

(2) Barkigia, K. M.; Chantranupong, L.; Smith, K. M.; Fajer, J. *J. Am. Chem. Soc.* **1988**, *110*, 7566.

(3) (a) Kadish, K. M.; Van Caemelbecke, E. V.; D'Souza, F. D.; Medforth, C. J.; Smith, K. M.; Tabard, A. *Organometallics* **1993**, *12*, 2411. (b) Kadish, K. M.; Van Caemelbecke, E. V.; Boulas, P.; D'Souza, F. D.; Vogel, E.; Kisters, M.; Medforth, C. J.; Smith, K. M. *Inorg. Chem.* **1993**, *32*, 4177.

(4) Gudowska-Nowak, E.; Newton, M. D.; Fajer, J. *J. Phys. Chem.* **1990**, *94*, 5795.

(5) Medforth, C. J.; Berber, M. D.; Smith, K. M.; Shelnutt, J. A. *Tetrahedron Lett.* **1990**, *31*, 3719.

(6) Shelnutt, J. A.; Medforth, C. J.; Berber, M. D.; Barkigia, K. M.; Smith, K. M. *J. Am. Chem. Soc.* **1991**, *113*, 4077.

(7) Jentzen, W.; Simpson, M. C.; Hobbs, J. D.; Song, X.-Z.; Ema, T.; Nelson, N. Y.; Medforth, C. J.; Smith, K. M.; Veyrat, M.; Mazzanti, M.; Ramasseul, R.; Marchon, J.-C.; Takeuchi, T.; Goddard, W. A., III; Shelnutt, J. A. *J. Am. Chem. Soc.* **1995**, *117*, 11 085.

(8) Schweitzer-Stenner, R. *Q. Rev. Biophys.* **1989**, *22*, 381.

(9) Berghuis, A. M.; Brayer, G. D. *J. Mol. Biol.* **1992**, *223*, 959.

(10) Hobbs, J. D.; Shelnutt, J. A. *J. Protein Chem.* **1995**, *14*, 19.

(11) Anderson, K. K.; Hobbs, J. D.; Luo, L.; Stanley, K. D.; Quirke, J. M. E.; Shelnutt, J. A. *J. Am. Chem. Soc.* **1993**, *115*, 12346.

(12) For example, the lowest-frequency normal mode γ_{14} of B_{1u} symmetry is calculated to be at 44 cm^{-1} for nickel(II) octaethylporphyrin [Ni(OEP)] (ref 28d). The comparison of the relative displacements of the macrocyclic atoms for this mode with the *ruf* deformation occurring in the X-ray crystal structures of the tetragonal crystalline forms of Ni(OEP) (ref 32) and nickel(II) *meso*-tetraphenylporphyrin [Ni(TPP)] (ref 34b) reveals that these relative displacements are almost identical.

(13) (a) Song, X.-Z.; Jentzen, W.; Jia, S.-L.; Jaquinod, L.; Nurco, D. J.; Medforth, C. J.; Smith, K. M.; Shelnutt, J. A. *J. Am. Chem. Soc.* **1996**, *118*, 12975. (b) Song, X.-Z.; Jaquinod, L.; Jentzen, W.; Jia, S.-L.; Ma, J.-G.; Nurco, D. J.; Medforth, C. J.; Smith, K. M.; Shelnutt, J. A., in preparation.

(14) Scheidt, W. R.; Lee, Y. J. *Struct. Bonding (Berlin)* **1987**, *64*, 1.

(15) Wilson, E. B.; Decius, J. C.; Cross, P. C. *Molecular Vibrations*; Dover: New York, 1980.

(16) The 24 displacement vectors $\Delta\hat{\vec{r}}_n$ of the *n*th macrocyclic atom defining the eigenvectors can be arranged in a one-column vector with 72 (= 24·3) entries. Thus, the first three elements are $\Delta\hat{x}_1$, $\Delta\hat{y}_1$, $\Delta\hat{z}_1$, and the next three are $\Delta\hat{x}_2$, $\Delta\hat{y}_2$, $\Delta\hat{z}_2$ and so on. The dot product between two vectors is defined in the usual way. However, the vectors $\Delta\hat{\vec{r}}_n$ can also be in a (24 × 3) matrix: the first column consists of 24 $\Delta\hat{x}_n$ coordinates, the second column of 24 $\Delta\hat{y}_n$ coordinates, and the last column of 24 $\Delta\hat{z}_n$ coordinates. In that case, the dot product is then given by $\mathrm{tr}(\hat{\mathbf{Q}}'^{\Gamma}_m\hat{\mathbf{Q}}^{\Gamma}_k)$, in which the symbol tr represents the trace of the matrix (sum of diagonal elements).

(17) (a) Medforth, C. J.; Senge, M. O.; Smith, K. M.; Sparks, L. D.; Shelnutt, J. A. *J. Am. Chem. Soc.* **1992**, *114*, 9859. (b) Shelnutt, J. A.; Majumder, S. A.; Sparks, L. D.; Hobbs, J. D.; Medforth, C. J.; Senge, M. O.; Smith, K.M.; Miura, M.; Quirke, J. M. E. *J. Raman Spectrosc.* **1992**, *23*, 523. (c) Hobbs, J. D.; Majumder, S. A.; Luo, L.; Sickelsmith, G. A.; Quirke, J. M.E.; Medforth, C. J.; Smith, K. M.; Shelnutt J. A. *J. Am. Chem. Soc.* **1994**, *116*, 3261. (d) Miura, M.; Majumder, S. A.; Hobbs, J. D.; Renner, M. W.; Furenlid, L. R.; Shelnutt, J. A. *J. Am. Chem. Soc.* **1994**, *33*, 6078.

(18) The nonbonded interactions consist of van der Waals and electrostatic terms. In our improved force field for metalloporphyrin (ref 13), the Lennard-Jones 12-6 type expression is used for describing van der Waals interactions except for hydrogen atoms for which the exponetial-6 type expression is used. The electrostatic (Coulomb) interactions result from monopole−monopole interactions of partial atomic charges (Rappé, A. K.; Goddard, W. A., III. *J. Phys. Chem.* **1991**, *95*, 3358). In calculating the electrostatic interactions for the charge distributions, the solvent dielectric constant was set to that of carbon disulfide (2.64). Furthermore, the masses used in the calculation for determining the non-mass-weighted atomic displacements of the normal-mode coordinates are for hydrogen, carbon, and nitrogen atoms 1.008, 12.011, and 14.007 amu, respectively, and the masses of the metals Cu and Ni are 58.700 and 63.540 amu, respectively.

(19) Schomaker, V.; Waser, J.; Marsh, R. E.; Bergman, G. *Acta Crystallogr.* **1959**, *12*, 600.

(20) (a) Luzzati, P. V. *Acta Crystallogr.* **1952**, *5*, 802. (b) Cruickshank, D. W. J. *Acta Crystallogr.* **1960**, *13*, 774.

(21) (a) Sparks, L. D.; Medforth, C. J.; Park, M.-S.; Chamberlain, J. R; Ondrias, M. R.; Senge, M. O.; Smith, K. M.; Shelnutt J. A. *J. Am. Chem. Soc.* **1993**, *115*, 581. (b) Sparks, L. D.; Anderson, K. K.; Medforth, C. J.; Smith, K. M.; Shelnutt, J. A. *Inorg. Chem.* **1994**, *33*, 2297.

(22) Medforth, C. J.; Muzzi, C. M.; Shea, K. M.; Smith, K. M.; Abraham, R. J.; Jia, S.-L.; Shelnutt, J. A. Submitted for publication.

(23) (a) Baldwin, J. L.; Chothia, C. *J. Mol. Biol.* **1979**, *129*, 175. (b) Plato, M.; Mobius, K.; Michel-Beyerle, M. E.; Bixon, M.; Jortner, J. *J. Am. Chem. Soc.* **1988**, *110*, 7279. (c) Alden, R. G.; Ondrias, M. R.; Shelnutt, J. A. *J. Am. Chem. Soc.* **1990**, *112*, 691.

(24) Senge, M. O.; Medforth, C. J.; Forsyth, T. P.; Lee, D. A.; Olmstead, M. M.; Jentzen, W.; Pandey, R. K.; Shelnutt, J. A.; Smith, K. M. *Inorg. Chem.* Submitted for publication.

(25) (a) Hoard, J. L. *Science* **1971**, *174*, 1295. (b) Hoard, J. L. *Ann. N. Y. Acad. Sci.* **1973**, *206*, 18.

(26) (a) Jentzen, W.; Song, X.-Z.; Jia, S.-L.; Shang, M.; Scheidt, W. R.; Shelnutt, J. A. Unpublished results. (b) Jentzen, W.; Turowska-Tyrk, I.; Scheidt, W. R.; Shelnutt, J. A. *Inorg. Chem.* **1996**, *35*, 3559.

(27) An example makes this point clearer. The static displacements along the out-of-plane A_{2u} mode γ_9 (32 cm^{-1}) of Ni(OEP) resemble the known *dom* deformation, whereas the second lowest-frequency A_{2u} mode γ_8 at 108 cm^{-1} looks like a sombrero-type distortion in which the metal displacement and the tilting of the four pyrrole planes are out-of-phase. [Figure 12 in the paper from Li and co-workers (ref 28d) illustrates this type of distortion.] Thus, the main difference between these modes is the in-phase (doming) and out-of-phase (sombrero) motion of the metal with respect to the macrocyclic atoms. Considering only the 24-atom macrocycle, the static displacements of these atoms, however, are very similar; therefore, they represent almost the same macrocyclic deformation type.

(28) (a) *Ab inito* calculations, Rohlfing, C.; Shelnutt, J. A. Unpublished results. (b) Warshel, A.; Lappicirella, A. *J. Am. Chem. Soc.* **1981**, *103*, 4664. (c) Li, X.-Y.; Czernuszewics, R. S.; Kincaid, J. R.; Su, Y. O.; Spiro, T. G. *J. Phys. Chem.* **1990**, *94*, 31. (d) Li, X.-Y.; Czernuszewicz, R. S.; Kincaid, J. R.; Spiro, T. G. *J. Am. Chem. Soc.* **1989**, *111*, 7012.

(29) If the displacements are lower than 2.0 Å for the *sad*, *ruf*, *dom*, and *pro* deformations and 1.0 Å for the *wav* deformation, the structural parameters depend almost linearly on the displacements. That is, the deviations between the calculated structural changes using the equations in the footnote of Table 1 (for larger deformations) and the estimated changes using the linear relationships are less than 5 %. The calculated structural changes are based on the reasonable assumption that the bond distances of the distorted structure are almost equal to the reference structure. Analogously, the structural changes for the in-plane deformations are also linearly dependent of the displacements assuming only that the *rot* displacement is less than 4 Å. As an example, using Tables 1 and 2, the estimated ruffling angle $C_\alpha N-C_\alpha$ is 32.0° [= (22.0 deg $Å^{-1}$) × (1.456 Å)], a value which is close to that observed one (32.8°) for the crystal structure of the tetragonal form of Ni(OEP) (refs 32, 26b).

(30) The frequencies $\tilde{\nu}^{\Gamma}_m$ are associated with the forces which are required to displace the macrocyclic atoms from their equilibrium configuration. Of course, the normal-mode frequencies vary depending on the nature of the peripheral substituents and the metal and axial ligands. These frequencies, however, change not because the forces within the macrocycle are significantly altered, but mainly because the masses, orientation, and nonbonding interactions of the attached substituents affect the frequencies.

(31) *3D Search and Research Using the Cambridge Structural Database.* Allen, F. H.; Kennard, O. *Chemical Design Automation News* **1993**, *8(1)*, 1, 31−37.

(32) Meyer, E. F. *Acta Crystallogr., Sect. B* **1972**, *28*, 2162.

(33) Fleischer, E. B.; Miller, C. K.; Webb, L. E. *J. Am. Chem. Soc.* **1964**, *86*, 2342.

(34) (a) Jentzen, W.; Unger, E.; Song, X.-Z.; Turowska-Tyrk, I.; Schweitzer-Stenner, R.; Dreybrodt, W.; Shelnutt, J. A. *J. Phys. Chem.*, submitted for publication. (b) Jentzen, W.; Song, X.-Z.; Turowska-Tyrk, I.; Scheidt, W. R.; Shelnutt, J. A. In preparation.

(35) Ema, T.; Senge, M. O.; Nelson, N. Y.; Ogoshi, H.; Smith, K. M. *Angew. Chem., Int. Ed. Engl.* **1994**, 33, 1879.

(36) Barkigia, K. M.; Renner, M. W.; Furenlid, L. R.; Medforth, C. J.; Smith, K. M.; Fajer, J. *J. Am. Chem. Soc.* **1993**, *115*, 3627.

(37) Cullen, D. L.; Meyer, E. F. *J. Am. Chem. Soc.* **1974**, *96*, 2095.

(38) Brennan, T. D.; Scheidt, W. R.; Shelnutt, J. A. *J. Am. Chem. Soc.* **1988**, *110*, 3919.

(39) Pace, L. J.; Ullman, A.; Ibers, J. A. *Inorg. Chem.* **1982**, *21*, 199.

(40) Nurco, D. J.; Jaquinod, L.; Smith, K. M. Unpublished result.

(41) Nagata, T.; Osuka, A.; Maruyama, K.; Toriumi, K. *Acta Crystallogr. Sect. C: (Cryst. Struct. Commun.)* **1990**, *46*, 1745.

(42) Senge, M. O.; Ruhlandt-Senge, K.; Regli, K. J.; Smith, K. M. *J. Chem. Soc., Dalton Trans.* **1993**, 3519.

(43) Mazzanti, M.; Marchon, J.-C.; Shang, M.; Scheidt, W. R.; Jia, S.-L.; Shelnutt, J. A. *Science*, submitted for publication.

(44) Inniss, D.; Soltis, S. M.; Strouse, C. E. *J. Am. Chem. Soc.* **1988**, *110*, 5644.

(45) Iimura, Y.; Sakurai, T.; Yamamoto, K. *Bull. Chem. Soc. Jpn.* **1988**, 61, 821.

(46) Chen, B. M. L.; Tulinsky, A. *J. Am. Chem. Soc.* **1972**, *94*, 4144.

(47) Lauher, J. W.; Ibers, J. A. *J. Am. Chem. Soc.* **1973**, *95*, 1973.

(48) Nurco, D. J.; Medforth, C. J.; Forsyth, T. P.; Olmstead, M. M.; Smith, K. M. *J. Am. Chem. Soc.* **1996**, *118*, 10918.

(49) Hamilton, W. C. *Acta Crystallogr., Sect. A* **1969**, *25*, 194.

(50) Generally, the mean positional error for the X-ray crystal structures of synthetic porphyrins in three dimensions is about 0.006 Å when the final conventional discrepancy factor (*R*-value) is 0.07. However, in one (out-of-plane) and two dimensions (in-plane), these errors are 0.0030 and 0.0047 Å, respectively, assuming a Gaussian-distributed probability density function for the deviations (see Appendix C of the Supporting Information).

(51) The middle molecule in this trimer is placed between two others in a small laterally shifted sandwich-like configuration. The metal of the top molecule is positioned over the nitrogen (N1) of the middle molecule, whereas the metal of the bottom molecule is located directly below the opposite nitrogen (N3) of the middle molecule. (Figure S5 in the Supporting Information illustrates the crystal packing arrangement.) Further, each of these nitrogen atoms of the middle molecule is displaced out-of-plane toward the adjacent zinc ion. The resulting distortion of the middle molecule resembles the *wav* deformation. Since the distortion is very small, it would be expected that the distortion can be described adequately with the minimal basis. The structural decomposition results for the top, middle, and bottom Zn(P) molecules are listed in Table 2. The middle molecule exhibits a small, pure *wav*(*x*) deformation whereas the top and bottom molecules are mixtures of smaller contributions of *wav*(*x*) and other deformation types. An important point is that the *wav* deformation of the middle molecule cannot be described with only the minimal basis, as indicated by the large deviation between the total observed and simulated distortions. Indeed, the second lowest-

frequency normal coordinate of symmetry type E_g is required; that is, a normal deformation along $\hat{\mathbf{D}}_2^{Eg(x)}$. The displacements for the extended basis are given in the footnote of Table 2. Clearly, this distortion of the middle molecule of the Zn(P) trimer configuration is caused mainly by the localized axial metal−nitrogen interactions.

(52) Jentzen, W.; Shelnutt, J. A. *J. Am. Chem. Soc.* Submitted for publication.

(53) (a) Matsuura, Y.; Takano, T.; Dickerson, R. E. *J. Mol. Biol.* **1982**, *156*, 389 (451C). (b) Hartmann, H.; Steigemann, W.; Reuscher, H.; Parak, F. *Eur. Biophys. J.* **1987**, *14*, 337.

(54) (a) Fermi, G.; Perutz, M. F.; Shaanan, B.; Fourme, R. *J. Mol. Biol.* **1984**, *175*, 159. (b) Fronticelli, C.; Pechik, I.; Brinigar, W. S.; Kowalczyk, J.; Gilliland, G. L. *J. Biol. Chem.* **1994**, *269*, 23 965. (c) Liddington, R; Derewenda, Z.; Dodson, E.; Hubbard, R.; Dodson, G. *J. Mol. Biol.* **1992**, *228*, 551. (d) Kavanaugh, J. S.; Rogers, P. H.; Case, D. A.; Arnone, A. *Biochemistry* **1992**, *31*, 4111.

(55) The displacements were obtained by orienting the macrocycle with its peripheral substituents according to Figure 4 (panel A). The fifth ligand, histidine, is located above the mean plane. The resolution of the X-ray crystal structures and PDB reference codes are also given. 2HHB: refinement presenting the best estimate of the atomic coordinates, 1.7 Å (ref 54a). 3HHB: symmetry-averaged refinement, 1.7 Å (ref 54a). 4HHB: unrestrained refinement which are useful for statistical studies, 1.7 Å (ref 54a). 2HHD: 2.2 Å (ref 54b). 1HGA: 2.1 Å (ref 54c). 1HBB: low-salt crystal structure, 1.9 Å (ref 54d).

(56) (a) Bernstein, F. C.; Koetzle, T. F.; Williams, G. J. B.; Meyers, E. F.; Brice, M. D.; Rodgers, J. R.; Kennard, O.; Shimanouchi, T.; Tasumi, M. *J. Mol. Biol.* **1977**, *112*, 535. (b) Abola, E. E.; Bernstein, F. C.; Bryant, S. H.; Koetzle, T. F.; Weng, J. Brookhaven Protein Data Bank. In *Crystallographic Databases*−*Information Content, Software Systems, Scientific Applications;* Allen, F. H., Bergerhoff, G., Sievers, R., Eds.; Data Commission of The International Union of Crystallography: Bonn, Cambridge, Chester, **1987**; p 107. (c) Stampf, D. R.; Felder, C. E.; Sussman, J. L. *Nature* **1995**, *374*, 572.

(57) (a) Lindström, T. R.; Ho, C. *Proc. Natl. Acad. Sci. U.S.A.* **1972**, *69*, 1707. (b) Huestis, W. H.; Raftery, M. A. *Biochemistry* **1973**, *12*, 2531. (c) Huestis, W. H.; Raftery, M. A. *Biochemistry* **1975**, *14*, 1886.

(58) (a) Louie, G. V.; Brayer, G. D. *J. Mol. Biol.* **1990**, *214*, 527. (b) Berghuis, A. M.; Guillemette, J. G.; McLendon, G.; Sherman, F.; Smith, M.; Brayer, G. D. *J. Mol. Biol.* **1994**, *236*, 786. (c) Berghuis, A. M.; Guillemette, J. G.; Smith, M.; Brayer, G. D. *J. Mol. Biol.* **1994**, *235*, 1326. (d) Lo, T. P.; Guillemette, J. G.; Louie, G. V.; Smith, M.; Brayer, G. D. *Biochemistry* **1995**, *34*, 163. (e) Lo, T. P.; Murphy, M. E. P.; Guillemette, J. G.; Smith, M.; Brayer, G. D. *Protein Sci.* **1995**, *4*, 198. (f) Lo, T. P.; Komar-Panicucci, S.; Sherman, F.; McLendon, G.; Brayer, G. D. *Biochemistry* **1995**, *34*, 5259. (g) Murphy, M. E. P.; Fetrow, J. S.; Burton, R. E.; Brayer, G. D. *Protein Sci.* **1993**, *2*, 1429.

(59) Shelnutt, J. A.; Rousseau, D. L.; Dethmers, J. K.; Margoliash, E. *Biochemistry* **1981**, *20*, 6485.

(60) Dayhoff, M. O.; Eck, R. V. *Atlas of Protein Sequence and Structures*; Biomedical Research Foundation: Washington, DC, **1972**.

(61) The displacements were obtained by orienting the macrocycle with its peripheral substituents according to Figure 4 (panel C). Axial ligand, His-18, is located below the mean plane. The amino acid residues between the covalently bonded cysteines are Leu and Gln. The resolution of the X-ray crystal structures and PDB reference codes are also given. Wild type: 1.2 Å, ref 58a (1YCC). N52I: 1.9 Å, ref 58b (1CRH). N52I, C102T: 2.0 Å, ref 58b (1CRG). Y67F, C102T: 1.9 Å, ref 58c (1CTZ). Mutation Tyr-67 alters the local heme environment. F82Y, C102T: 2.0 Å, ref 58d (1CHH). L85M, C102T: 1.9 Å, ref 58e (1CSW). L85A, C102T: 1.9 Å, ref 58d (1CHJ). L85C, C102T: 1.8 Å, ref 58e (1CSU). L85F, C102T: 1.8 Å, ref 58e (1CSV). L94S, C102T: 1.9 Å, ref 58e (1CSX). R38A, F82S, C102A: 1.9 Å, ref 58f (1CIF). N52I, F82S, C102A: 1.8 Å, ref 58f (1CIE). N52I, Y67F, C102T: 2.1 Å, ref 58b (1CRJ). F82Y, L85A, C102T: 2.0 Å, ref 58d (1CHI). E21D, K22Q, P25A, H26N: 1.9 Å, ref 58g (1RAQ). E21D, K22Q, P25A, H26N: 2.3 Å, ref 58g (1RAP). R38A, N52I, F82S, C102A: 1.8 Å, ref 58f (1CIH).

(62) (a) Takano, T.; Dickerson, R. E. *J. Mol. Biol.* **1981**, *153*, 79. (b) Takano, T.; Dickerson, R. E. *J. Mol. Biol.* **1981**, *153*, 95.

(63) Ochi, H.; Hata, Y.; Tanaka, N.; Kakudo, M.; Sakurai, T.; Aihara, S.; Morita, Y. *J. Mol. Biol.* **1983**, *166*, 407.

(64) Sayle, R.; Milner-White, E. J. *Trends in Biochem. Sci.* **1995**, *20*, 333, No. 9.

(65) (a) Morimoto, Y.; Tani, T.; Okumura, H.; Higuchi, Y.; Yasuoka, N. *J. Biochem. (Tokyo)* **1991**, *110*, 532. (b) Higuchi, Y.; Kusunoki, M.; Matsuura, Y.; Yasuoka, N.; Kakudo, M. *J. Mol. Biol.* **1984**, *172*, 109. (c) Morais, J.; Palma, P. N.; Frazao, C.; Caldeira, J.; Moura, I.; LeGall, J.; Moura, J. J. G.; Carrondo, M. A. *Biochemistry* **1995**, *34*, 12 830. (d) Czjzek, M.; Payan, F.; Guerlesquin, F.; Bruschi, M.; Haser, R. *J. Mol. Biol.* **1994**, *243*, 653.

(66) The displacements were obtained by orienting the macrocycle with its peripheral substituents according to Figure 4 (panel C). The resolution of the X-ray crystal structures and PDB reference codes are also given. Hildenb.: *Desulfovibrio vulgaris*, strain Hildenborough, 2.0-Å resolution, ref 65a (2CYM). Miyaz.: *D. vulgaris*, strain Miyazaki, 1.8-Å resolution, ref 65b (2CDV). ATCC: *D. desulfuricans*, strain ATCC 27 774, 1.75-Å resolution, ref 65c (2CYR). Norw.: *D. desulfuricans*, strain Norway, 1.7-Å resolution, ref 65d (2CY3).

(67) The total observed distortions are in average for all hemes 1, hemes 2, and hemes 3 0.83(5), 0.98(16), and 0.51(15) Å, respectively (the values in parentheses are the standard deviations). The overall distortion for hemes 4 excluding the Norway strains are 1.17(8) Å. Finally, the total observed distortion for heme 4 from Norway strain is 0.8 Å. The mean deviation $\bar{\delta}_{oop,1}$ between the observed and simulated distortion is 0.034(19) Å for all heme groups.

(68) Ma, J.-G.; Jentzen, W.; Vanderkoi, J.; Song, X.-Z.; Jia, S.-L.; Hobbs, J. D.; Shelnutt, J. A. In preparation.

(69) (a) Timkovich, R.; Dickerson, R. E. *J. Mol. Chem.* **1976**, *251*, 2197. (b) Matsuura, Y.; Takano, T.; Dickerson, R. E. *J. Mol. Biol.* **1982**, *156*, 389. (c) Nakagawa, A.; Higuchi, Y.; Yasuoka, N.; Katsube, Y.; Yagi, T. *J. Biochem. (Tokyo)* **1990**, *108*, 701. (d) Murphy, M. E. P.; Nall, B. T.; Brayer, G. D. *J. Mol. Biol.* **1992**, *227*, 160. (e) Dobbs, A. J.; Faber, H. R.; Anderson, B. F.; Baker E. N. *Acta Crystallogr., Sect. D* **1996**, *52*, 356. (f) Deisenhofer, J.; Michel, H. *Science* **1989**, *245*, 1463. (g) Li, H.; Poulos, T. L. *Acta Crystallogr., Sect. D* **1995**, *51*, 21. (h) Durley, R. C. E.; Mathews, F. S. *Acta Crystallogr., Sect. D* **1996**, *52*, 65. (i) Finzel, B. C.; Poulos, T. L.; Kraut, J. *J. Biol. Chem.* **198**4, *259*, 13 027. (j) Xia, Z.; Mathews, F. S. *J. Mol. Biol.* **1990**, *212*, 837. (k) Yang, F.; Phillips, G. N. *J. Mol. Biol.* **1996**, *256*, 762.

(70) The displacements were obtained by orienting the macrocycle with its peripheral substituents according to Figure 4 (panel C). In the following, the location of the histidine with respect to the mean plane is indicated by a "+" (above) and a "−" sign (below). The resolution of the X-ray crystal structures, PDB reference codes, and the amino acid residues between the covalently bonded cysteines are also given if applicable. Cyt. *c*550 (2.5 Å): *Paracoccus denitrificans*/ATCC 13543, His (−), Lys-Ala, ref 69a (155C). Cyt. *c*551 (1.6 Å): *Pseudomonas aeruginosa*, His (−), Val-Ala, ref 69b (451C). Cyt. *c*553 (1.8 Å): *Desulfovibrio vulgaris*, strain Miyazaki, His (−), Val-Gly, ref 69c (1C53). Cyt. *c* iso-2 (1.9 Å): Baker's yeast isozyme 2, His (−), Gln-Gln, ref 69d (1YEA). Cyt. *c*′ (1.8 Å): *Alcaligenes sp*, strain NCIB 11015, His (−), Lys-Ala, ref 69e (1CGO). RC (2.3 Å): cytochrome unit of the reaction center *Rhodopseudomonas viridis*, sixth ligands (+) are for heme 1 (Thr-Tyr), heme 2 (Tyr-Thr), and heme 3 (Thr-Phe) methionine and for heme 4 histidine-124 (Arg-Thr), ref 69f (1PRC). Cyt. P450 (2.0 Å): *Bacillus megaterium*, sulfur (+), ref 69g (2BMH). Cytochrome P450 is a dimer of two identical chains A and B both having water as sixth axial ligand to the heme iron. Decomposition result of the heme group in chain A is shown. Bovine b_5 (1.5 Å): cytochrome b_5, *Bos taurus* (liver) His-39 (+), ref 69h (1CYO). Cyt. *c* perox. (1.7 Å): Baker's yeast (*Saccharomyces cerevisiae*), His (−), ref 69i (2CYP). Flavocyt. b_2 (2.4 Å): yeast flavocytochrome b_2 , His-43 (+), ref 69j (1FCB). Deoxymyoglobin (1.7 Å): sperm whale, His (+), pH 6.0, ref 69k (1VXG).

(71) The total nonplanar distortions range from 0.3 to 0.8 Å, while the individual contributions vary from −0.5 to 0.6 Å for *sad*, −0.2 to 0.6 Å for *ruf*, −0.3 to 0.3 Å for *dom*, and −0.2 to 0.4 Å for the *wav*(*x*) and *wav*(*y*) deformations. Again, no significant *pro* deformation is observed because it requires a much greater expenditure of energy by the protein, and therefore much smaller deformation of this type is likely to be observed in the structures of the heme groups.